

## Analysis and application of a lower envelope method for sharp-interface multiphase problems\*

by

**Antoine Laurain**

Faculty of Mathematics, University of Duisburg-Essen,  
Thea-Leymann-Str. 9, 45127 Essen, Germany  
antoine.laurain@uni-due.de

**Abstract:** We introduce and analyze a lower envelope method (LEM) for the tracking of motion of interfaces in multiphase problems. The main idea of the method is to define the phases as the regions where the lower envelope of a set of functions coincides with exactly one of the functions. We show that a variety of complex lower-dimensional interfaces naturally appear in the process. The evolution of phases is then achieved by solving a set of transport equations. In the first part of the paper, we show several theoretical properties, give conditions to obtain a well-posed behaviour, and show that the level set method is a particular case of the LEM. In the second part, we propose a LEM-based numerical algorithm for multiphase shape optimization problems. We apply this algorithm to an inverse conductivity problem with three phases and present several numerical results.

**Keywords:** lower envelope method, shape optimization, multiphase, sharp-interface problems, electrical impedance tomography

### 1. Introduction

The accurate modeling of multiple phases presenting sharp interfaces is highly relevant for physical phenomena and industrial processes. Examples of such problems are: optimization of the distribution of several materials in order to minimize certain costs and mechanical criteria in structural optimization (Mei and Wang, 2004; Vogiatzis et al., 2017; Wang and Wang, 2004; Wang et al., 2015; Zuo and Saitou, 2017), monitoring of multiphase fluid flow in oil recovery system (Liu et al., 2015), monitoring of sedimentation processes (Tossavainen et al., 2006), multiphase inverse problems (Liu et al., 2018; Tai and Chan,

---

\*Submitted: July 2024; Accepted: September 2024.

2004; Vese and Chan, 2002), and dry foams (Saye and Sethian, 2013; Weaire and Hutzler, 1999). On one hand, the level set method (LSM) (Osher and Sethian, 1988; Sethian, 1999), introduced by Osher and Sethian, has become a staple of sharp-interface modelling for two phases; see the recent review by Gibou, Fedkiw and Osher (2018). On the other hand, the case of three or more interfaces presents additional challenges and is an active field of research.

A variety of level set-based methods have been proposed to handle multi-phase algorithms in the literature. The color level set method (CLSM) has been introduced in Vese and Chan (2002) for image segmentation, see also Hintermüller and Laurain (2009), Mei and Wang (2004), Wang and Wang (2004). In this framework,  $n$  level set functions  $\varphi_1, \dots, \varphi_n$  are introduced, and for a given subset of indices  $I \subset \{1, \dots, n\}$  the corresponding phase is defined as  $\Omega_I := \{x \in \mathcal{D} \mid \varphi_i(x) < 0, \forall i \in I \text{ and } \varphi_j(x) > 0, \forall j \in \{1, \dots, n\} \setminus I\}$ . In this way, one can represent up to  $2^n$  phases. The multi-material level set-based method (MMLS), introduced in Wang et al. (2015), uses  $n$  level set functions to represent  $n + 1$  phases. The principle of the MMLS is similar to the CLSM, but the phases are defined using a different combination rule of functions. The reconciled level set method (RLSM), also known as the coupled level set method (Chen et al., 2010; Vogiatzis et al., 2017; Zhang, Chen and Osher, 2008), has been introduced in Merriman, Chen and Osher (1994) and is based on the diffusion of characteristic functions of each region. We also mention the piecewise constant level set (PCLS) method (Li and Tai, 2007), a projection method (Smith, Solis and Chopp, 2002), and a smoothed interface approach, using a signed distance function to enforce a fixed width of the transition layer, presented in Allaire et al. (2014).

These methods involve the use of multiple level set functions and, at times, additional procedures, such as projections, to prevent the formation of vacuums or overlaps. We observe that level set-based methods have a fundamental limitation when it comes to capturing the motion of triple points and multiple junctions using smooth functions, which originates from the fact that the level sets of a smooth function are in most cases smooth, and, consequently, the nonsmoothness of the phases at a multiple junction must come from another mechanism. In two dimensions, for instance, the triple points appearing in the methods mentioned above usually have one angle equal to  $\pi$  due to the smoothness of one of the phases at this junction point. This observation suggests the exploration of other paradigms than level set approaches to track the motion of multiple junctions and phases.

Another issue is that many of these approaches involve a small diffuse interface, or a regularization parameter to smoothen the level set functions. These regularization procedures introduce arbitrary parameters into the problem, which

need to be chosen ad hoc, may be unphysical, or need an asymptotic procedure to recover the sharp-interface configuration.

Among the level set-based methods, the Voronoi Implicit Interface Method (VIIM), Saye and Sethian (2011, 2013), is an exception as it is able to capture the motion of multiple junctions and complex interfaces using only one function for an entire multiphase system. However, it also involves taking the limit of  $\epsilon$ -smoothed solutions as  $\epsilon \rightarrow 0$ , which makes its analysis challenging; see Laurain (2017). Other methods, not based on level sets, include volume of fluid methods (Noh and Woodward, 1976), front tracking methods (Bronsard and Wetton, 1995), variational methods (Zhao et al., 2017), SIMP (Zuo and Saitou, 2017), an alternating active-phase algorithm (Tavacoli and Mohseni, 2014), and phase field models (Garcke, Nestler and Stoth, 2000), where a diffusive layer with positive thickness models the interface. The study of the sharp interface limit when the thickness of the diffusive layer tends to zero is an active field of research in the phase-field community; see Barret, Garcke and Nürnberg (2008) or Bronsard, Garcke and Stoth (1998).

In this paper, we introduce a lower envelope method (LEM) for tracking the motion of interfaces in multiphase problems. The LEM belongs to the class of implicit interface methods, but not to the class of level set methods, except for the particular case of two phases, where it coincides with the LSM. Regarding the issues discussed above, the LEM has the following advantages. It does not involve any regularization parameter or small diffuse interface, so the interfaces stay sharp at all times. By construction, it precludes the appearance of vacuum and overlaps, and naturally produces triple points and other nonsmooth interfaces using smooth functions. In particular, in two dimensions, we can show that the triple points have angles between 0 and  $\pi$ , which can be explicitly computed using the functions involved in the method. Since no regularization or asymptotic procedure is required in the LEM, the analysis of the motion of multiple junctions and complex interfaces becomes much more tractable.

We give now a brief overview of the main ideas of the LEM. Given a collection  $\phi$  of functions  $\phi_k$  in  $C^\infty(\mathbb{R}^d, \mathbb{R})$ ,  $k \in \mathcal{K} \subset \mathbb{N}$ , their lower envelope  $E_\phi$  is the supremum of the functions whose graph remains below the union of the graphs of the functions in  $\phi$ . By construction,  $E_\phi$  always coincides with one or more functions  $\phi_k$  at a point  $x$ . On the one hand,  $E_\phi$  is locally smooth at points where it coincides with exactly one function  $\phi_k$ . On the other hand, under certain natural conditions on  $\phi$  that will be discussed in detail,  $E_\phi$  is not smooth at points where it coincides with two or more functions  $\phi_k$ , and the regions where  $E_\phi$  coincides with exactly  $d_0$  functions  $\phi_k$ , where  $d_0 \leq d + 1$ , are sets of dimensions  $d - (d_0 - 1)$ . The main idea of the LEM is to exploit this key property of  $E_\phi$  by defining the phases as the sets where  $E_\phi$  coincides with one of the functions  $\phi_k$ . This naturally models a multiphase configuration with

nonsmooth phases and a variety of lower-dimensional interfaces and multiple junctions, such as triple points in two dimensions, quadruple points and triple lines in three dimensions. We show that the motion of these phases can be described by solving a set of transport equations, generalizing the main idea of the level set method for nonsmooth domains, described in Laurain and Sturm (2016).

The set of phases, defined by the lower envelope  $E_\phi$ , is called *minimization diagram* in computational geometry, see Edelsbrunner and Seidel (1986). Notable particular examples are Voronoi, Laguerre and power diagrams. Minimization diagrams have primarily been studied in the stationary case. Recently, the sensitivity analysis of parameterized minimization diagrams has been investigated in Birgin, Laurain and Menezes (2023). The present work extends that investigation by studying time-dependent minimization diagrams via transport equations, focusing on tracking interface motion in multiphase problems. In this way, it complements Birgin, Laurain and Menezes (2023), and together, both works contribute to building an abstract theory of evolving and parameterized minimization diagrams.

In this paper we describe the LEM in the framework of multiphase optimization problems involving PDEs, considered as shape optimization problems (Allaire, Dapogny and Jouve, 2021; Azegami, 2020; Delfour and Zolésio, 2011; Sokolowski and Zolésio, 1992). In shape optimization, the derivative of the cost functional can either be written in a weak form, often called distributed shape derivative, which is a volume integral when the cost function is itself a volume integral, or in a strong form, called boundary expression or Hadamard formula. Boundary expressions are often computed for domains, which are at least  $\mathcal{C}^1$ , even though they can sometimes be computed for Lipschitz or polygonal domains, but this requires a careful analysis of the regularity of solutions of the underlying PDEs; see Laurain (2019). Distributed shape derivatives, on the other hand, are usually valid for domains with lower regularity, such as curvilinear polygons, Lipschitz domains or even open sets. Since the sets involved in multiphase optimization problems with at least three phases are usually curvilinear polygons, distributed shape derivatives are a key ingredient of the LEM. Other advantages of shape derivatives in distributed form are their higher accuracy for numerical approximation; see Delfour, Payre and Zolésio (1995), Hiptmair, Paganini and Sargheini (2014), and the fact that shape derivatives written in strong form are sometimes impractical for numerical purposes, as they may involve the computation of jumps across interfaces; see the related discussions in Allaire et al. (2014), Laurain and Sturm (2016).

In order to show the feasibility and efficiency of the LEM, we present an application to the inverse problem of electrical impedance tomography (EIT) with three phases. In real-life problems, many applications of EIT involve multiple

phases and sharp interfaces. The incorporation of prior information about sharp interfaces explicitly in the modeling of the problem is especially advantageous for inverse problems, as they are characterized by incomplete data; see Liu et al. (2015). Sharp-interface models for EIT with two phases have been studied in Albuquerque, Laurain and Sturm (2020), Beretta, Francini and Vessella (2017), Beretta et al. (2018), Hintermüller and Laurain (2008), Hintermüller, Laurain and Novotny (2002), Laurain and Sturm (2016), and Tai and Chan (2004), but there are fewer references for three phases or more, we mention Liu et al. (2018) for a parametric level set method, and Liu et al. (2015) for multi-phase flow monitoring. In this paper we compute the distributed shape derivative for a general multiphase anisotropic EIT problem with piecewise smooth conductivity. For the numerical experiments we consider the particular case of three phases and isotropic conductivity.

The paper is organized as follows. In Section 2 we define the lower envelope and the phases, study the properties of the phases distribution and give several examples. In particular, we give a natural condition on the functions so that the phase distribution defines a partition of the domain without overlapping, which is a crucial property for the proper functioning of the algorithm. In Section 3, we define and discuss properties of weak and strong forms of shape derivatives in the multiphase setting. In Section 4, we demonstrate how the motion of phases, interfaces and multiple junctions can be tracked using transport equations, discuss the possibility of reducing the dimension of perturbation fields, introduce the LEM, and show that the level set method, Osher and Sethian (1988), Sethian (1999), is a particular case of the LEM. In Section 5 we study geometric properties of the LEM, in particular, we compute the angles at a triple junction in two dimensions, and we verify that multiple junctions evolve with the expected velocity. In Section 6 we apply the LEM to a multiphase EIT problem and present several numerical experiments.

## 2. Multiphase setting using a lower envelope function

In this section we introduce the multiphase setting based on a lower envelope approach. The main task is to study the geometric properties of the phases and to give conditions on the lower envelope functions in order to avoid phase overlaps and obtain a partition of the domain.

Let  $d \geq 2$  and  $\mathcal{D} \subset \mathbb{R}^d$  be open and bounded. Define the set of indices

$$\mathcal{K} := \{0, 1, \dots, \kappa - 1\} \subset \mathbb{N},$$

where  $\kappa$  is the cardinal of  $\mathcal{K}$ , and  $\mathbb{I}_k^r := \{\mathcal{I} \subset \mathcal{K} \mid |\mathcal{I}| = r \text{ and } \mathcal{I} \ni k\}$ . Let  $\phi = (\phi_0, \phi_1, \dots, \phi_{\kappa-1}) \in \mathcal{C}^\infty(\mathbb{R}^d, \mathbb{R}^\kappa)$ . We will use the notation  $D\phi$  for the Jacobian matrix of  $\phi$ .

DEFINITION 1 *The function*

$$E_\phi(x) := \min_{k \in \mathcal{K}} \phi_k(x) \quad (1)$$

is called *lower envelope of  $\phi$* . We define the open sets

$$\Omega_k(\phi) := \text{int}\{x \in \mathcal{D} \mid \phi_k(x) = E_\phi(x)\}, \quad \text{for } k \in \mathcal{K}, \quad (2)$$

or equivalently

$$\Omega_k(\phi) := \text{int}\{x \in \mathcal{D} \mid \phi_k(x) \leq \phi_\ell(x), \forall \ell \in \mathcal{K} \setminus \{k\}\}, \quad \text{for } k \in \mathcal{K}. \quad (3)$$

The sets  $\Omega_k(\phi)$  are called “*phases*”. We denote by  $\mathbf{\Omega}(\phi) := (\Omega_0(\phi), \dots, \Omega_{\kappa-1}(\phi))$  the vector of phases  $\Omega_k(\phi)$ .

The set of phases  $\{\Omega_k(\phi)\}_{k \in \mathcal{K}}$  is called *minimization diagram* in computational geometry, see Edelsbrunner and Seidel (1986). The following lemma describes several important properties of the phases  $\Omega_k(\phi)$ .

LEMMA 1 *For all  $k \in \mathcal{K}$  we have*

$$\{x \in \mathcal{D} \mid \phi_k(x) < \phi_\ell(x), \forall \ell \in \mathcal{K} \setminus \{k\}\} \subset \Omega_k(\phi). \quad (4)$$

Moreover, for all  $k \in \mathcal{K}$  we have

$$\overline{\Omega_k(\phi)} = \{x \in \overline{\mathcal{D}} \mid \phi_k(x) \leq \phi_\ell(x), \forall \ell \in \mathcal{K} \setminus \{k\}\} \quad (5)$$

and

$$\bigcup_{k \in \mathcal{K}} \overline{\Omega_k(\phi)} = \overline{\mathcal{D}}. \quad (6)$$

PROOF The set  $\{x \in \mathcal{D} \mid \phi_k(x) < \phi_\ell(x), \forall \ell \in \mathcal{K} \setminus \{k\}\}$  is open, since it is the preimage of an open set under the vector-valued continuous function

$$(\phi_k - \phi_0, \phi_k - \phi_1, \dots, \phi_k - \phi_{k-1}, \phi_k - \phi_{k+1}, \dots, \phi_k - \phi_{\kappa-1}) \in \mathcal{C}^\infty(\mathbb{R}^d, \mathbb{R}^{\kappa-1}).$$

Since we clearly have the inclusion

$$\{x \in \mathcal{D} \mid \phi_k(x) < \phi_\ell(x), \forall \ell \in \mathcal{K} \setminus \{k\}\} \subset \{x \in \mathcal{D} \mid \phi_k(x) \leq \phi_\ell(x), \forall \ell \in \mathcal{K} \setminus \{k\}\},$$

and  $\Omega_k(\phi)$  is, by definition, the largest open set included in

$$\{x \in \mathcal{D} \mid \phi_k(x) \leq \phi_\ell(x), \forall \ell \in \mathcal{K} \setminus \{k\}\},$$

(4) follows.

Now, taking the closure of both sets in (4), we obtain

$$\{x \in \overline{\mathcal{D}} \mid \phi_k(x) \leq \phi_\ell(x), \forall \ell \in \mathcal{K} \setminus \{k\}\} \subset \overline{\Omega_k(\phi)}. \quad (7)$$

Considering definition (3), we also have

$$\Omega_k(\phi) \subset \{x \in \mathcal{D} \mid \phi_k(x) \leq \phi_\ell(x), \forall \ell \in \mathcal{K} \setminus \{k\}\}. \quad (8)$$

Taking the closure of both sets in (8), we obtain

$$\overline{\Omega_k(\phi)} \subset \{x \in \overline{\mathcal{D}} \mid \phi_k(x) \leq \phi_\ell(x), \forall \ell \in \mathcal{K} \setminus \{k\}\}. \quad (9)$$

By gathering (7) and (9), we obtain (5).

The inclusion  $\bigcup_{k \in \mathcal{K}} \overline{\Omega_k(\phi)} \subset \overline{\mathcal{D}}$  in (6) is clear, since  $\overline{\Omega_k(\phi)}$  are subsets of  $\overline{\mathcal{D}}$ . Conversely, take  $x \in \overline{\mathcal{D}}$  and  $k \in \operatorname{argmin}_{\ell \in \mathcal{K}} \phi_\ell(x) \neq \emptyset$ . Then, in view of (5), we have  $x \in \overline{\Omega_k(\phi)}$ , which proves that  $\overline{\mathcal{D}} \subset \bigcup_{k \in \mathcal{K}} \overline{\Omega_k(\phi)}$ . Thus, we obtain (6). ■

Without additional restrictions on  $\phi$ , the sets  $\Omega_k(\phi)$  may overlap, which is an undesirable behaviour. This situation can be prevented by using the proper assumptions on  $\phi$  that we describe further. We start with several definitions.

**DEFINITION 2** *Let  $\mathcal{I} = \{k_1, k_2, \dots, k_{|\mathcal{I}|}\} \subset \mathcal{K}$ , where the cardinal  $|\mathcal{I}|$  of  $\mathcal{I}$  satisfies  $2 \leq |\mathcal{I}| \leq \kappa$  and  $k_i < k_{i+1}$ ,  $1 \leq i \leq |\mathcal{I}| - 1$ . Define*

$$\widehat{\phi}_{\mathcal{I}} := (\widehat{\phi}_1, \widehat{\phi}_2, \dots, \widehat{\phi}_{|\mathcal{I}|-1}) \in \mathcal{C}^\infty(\mathbb{R}^d, \mathbb{R}^{|\mathcal{I}|-1})$$

with  $\widehat{\phi}_i := \phi_{k_1} - \phi_{k_{i+1}}$  for  $1 \leq i \leq |\mathcal{I}| - 1$ . Define also

$$\begin{aligned} \mathcal{M}_{\mathcal{I}}(\phi) &:= \{x \in \overline{\mathcal{D}} \mid \widehat{\phi}_{\mathcal{I}}(x) = 0\} \\ &= \{x \in \overline{\mathcal{D}} \mid \phi_{k_i}(x) = \phi_{k_j}(x), \text{ for all } 1 \leq i, j \leq |\mathcal{I}| \text{ and } i \neq j\}, \end{aligned} \quad (10)$$

$$\mathcal{E}_{\mathcal{I}}(\phi) := \bigcap_{k \in \mathcal{I}} \partial \Omega_k(\phi), \quad (11)$$

where  $\partial \Omega_k(\phi)$  denotes the boundary of  $\Omega_k(\phi)$  in  $\mathbb{R}^d$ .

The set  $\mathcal{E}_{\mathcal{I}}(\phi)$  is the set of interfaces, shared by all the phases  $\Omega_k(\phi)$ , whose index  $k$  belongs to  $\mathcal{I}$ . We will see that the set  $\mathcal{M}_{\mathcal{I}}(\phi)$  is, roughly speaking, the union of  $\mathcal{E}_{\mathcal{I}}(\phi)$  and some “ghost” interfaces that will be useful for the analysis; see Examples 1 and 4 further on in this section. Our aim is to avoid the situation, where  $\mathcal{M}_{\mathcal{I}}(\phi)$  is “thick”, i.e., the dimension of  $\mathcal{M}_{\mathcal{I}}(\phi)$  should be at most  $d - (|\mathcal{I}| - 1)$  when  $|\mathcal{I}| \leq d$ , otherwise differentiability issues would arise when defining the LEM. This property can be guaranteed by imposing the proper condition on  $D\widehat{\phi}_{\mathcal{I}}$ .

LEMMA 2 *Let  $\mathcal{I} \subset \mathcal{K}$ ,  $2 \leq |\mathcal{I}| \leq d$ , then we have*

$$\mathcal{E}_{\mathcal{I}}(\phi) \subset \mathcal{M}_{\mathcal{I}}(\phi). \quad (12)$$

*In addition, assume  $D\widehat{\phi}_{\mathcal{I}}(x)$  has maximal rank  $|\mathcal{I}| - 1$  for all  $x \in \mathcal{M}_{\mathcal{I}}(\phi)$ . Then,  $\mathcal{M}_{\mathcal{I}}(\phi)$  is the intersection of a  $\mathcal{C}^{\infty}$ -manifold of dimension  $d - (|\mathcal{I}| - 1)$  with  $\overline{\mathcal{D}}$ .*

PROOF In view of definition (10), we have

$$\mathcal{M}_{\mathcal{I}}(\phi) = \bigcap_{\mathcal{I}_2 \subset \mathcal{I}, |\mathcal{I}_2|=2} \mathcal{M}_{\mathcal{I}_2}(\phi). \quad (13)$$

Then, for all  $\mathcal{I}_2 = \{k, \ell\} \subset \mathcal{I}$  with  $k \neq \ell$ , we have the property

$$\partial\Omega_k(\phi) \cap \partial\Omega_{\ell}(\phi) \subset \mathcal{M}_{\mathcal{I}_2}(\phi). \quad (14)$$

Indeed, let  $x \in \partial\Omega_k(\phi) \cap \partial\Omega_{\ell}(\phi)$ , then, in view of (5), we have, in particular,  $\phi_k(x) \leq \phi_{\ell}(x)$  and  $\phi_{\ell}(x) \leq \phi_k(x)$ . Thus,  $\phi_k(x) = \phi_{\ell}(x)$ , which implies  $x \in \mathcal{M}_{\mathcal{I}_2}(\phi)$ . Then, using (13) we obtain (12).

Next, due to (10) we have  $\mathcal{M}_{\mathcal{I}}(\phi) = \widehat{\phi}_{\mathcal{I}}^{-1}(\{0\}) \cap \overline{\mathcal{D}}$  and since, by assumption,  $D\widehat{\phi}_{\mathcal{I}}(x)$  has rank  $|\mathcal{I}| - 1$  for all  $x \in \mathcal{M}_{\mathcal{I}}(\phi)$ , then 0 is a regular value of  $\widehat{\phi}_{\mathcal{I}}|_{\overline{\mathcal{D}}}$ . This shows that  $\mathcal{M}_{\mathcal{I}}(\phi) = \widehat{\phi}_{\mathcal{I}}^{-1}(\{0\}) \cap \overline{\mathcal{D}}$  is a  $\mathcal{C}^{\infty}$ -manifold of dimension  $d - (|\mathcal{I}| - 1)$ . ■

Note that (12) and (14) are only inclusions in general, this is illustrated in Example 1. Indeed, in view of (2) it may happen that  $x$  satisfies  $\phi_j(x) = \phi_k(x) > \phi_{\ell}(x) = E_{\phi}(x)$  for some pairwise distinct indices  $j, k, \ell$ , which would imply  $x \in \mathcal{M}_{\{j,k\}}(\phi)$  even though  $x \notin \partial\Omega_j(\phi) \cap \partial\Omega_k(\phi)$ . In this sense,  $\mathcal{M}_{\mathcal{I}}(\phi)$  contains the “ghost” interfaces  $\mathcal{M}_{\mathcal{I}}(\phi) \setminus \mathcal{E}_{\mathcal{I}}(\phi)$ .

We now give a condition that guarantees the non-overlapping of the phases  $\Omega_k(\phi)$ .

PROPOSITION 1 *Let  $\{k, \ell\} \subset \mathcal{K}$  with  $k \neq \ell$ . If  $|\nabla(\phi_k - \phi_{\ell})| > 0$  on  $\mathcal{M}_{\{k,\ell\}}(\phi)$ , then we have*

$$\Omega_k(\phi) \cap \Omega_{\ell}(\phi) = \emptyset. \quad (15)$$

PROOF Assume that there exists  $x \in \Omega_k(\phi) \cap \Omega_{\ell}(\phi)$ . Since  $\Omega_k(\phi)$  and  $\Omega_{\ell}(\phi)$  are open, there exists an open ball  $B(x, r)$  of center  $x$  and radius  $r > 0$ , such that  $B(x, r) \subset \Omega_k(\phi) \cap \Omega_{\ell}(\phi)$ . Then, in view of (3), we have for all  $y \in B(x, r)$  that  $\phi_k(y) \leq \phi_{\ell}(y)$  and  $\phi_{\ell}(y) \leq \phi_k(y)$ , which yields  $\phi_k(y) = \phi_{\ell}(y)$ . Thus, we have  $B(x, r) \subset \mathcal{M}_{\{k,\ell\}}(\phi)$  and, consequently,  $D\widehat{\phi}_{\{k,\ell\}}(y) = \nabla(\phi_k - \phi_{\ell})(y) = 0$  for all  $y \in B(x, r)$ , which contradicts the hypothesis that  $|\nabla(\phi_k - \phi_{\ell})| > 0$  on  $\mathcal{M}_{\{k,\ell\}}(\phi)$ . Hence, (15) follows. ■

The purpose of the next lemma is to give a characterization of the phase boundary  $\partial\Omega_k(\phi)$  in terms of the sets  $\mathcal{E}_{\mathcal{I}}(\phi)$ . This result is further employed in Section 4 to model the motion of the interfaces  $\partial\Omega_k(\phi)$  using  $\phi$ .

LEMMA 3 *For all  $k \in \mathcal{K}$  we have*

$$\mathcal{D} \cap \bigcup_{\mathcal{I} \in \mathbb{I}_k^2} \mathcal{E}_{\mathcal{I}}(\phi) = \mathcal{D} \cap \bigcup_{\mathcal{I} \in \mathbb{I}_k^+, r \geq 2} \mathcal{E}_{\mathcal{I}}(\phi) \subset \mathcal{D} \cap \partial\Omega_k(\phi). \quad (16)$$

If, in addition,  $|D\widehat{\phi}_{\mathcal{I}}| > 0$  on  $\mathcal{M}_{\mathcal{I}}(\phi)$  for all  $\mathcal{I} \in \mathbb{I}_k^2$ , then

$$\mathcal{D} \cap \bigcup_{\mathcal{I} \in \mathbb{I}_k^2} \mathcal{E}_{\mathcal{I}}(\phi) = \mathcal{D} \cap \bigcup_{\mathcal{I} \in \mathbb{I}_k^+, r \geq 2} \mathcal{E}_{\mathcal{I}}(\phi) = \mathcal{D} \cap \partial\Omega_k(\phi). \quad (17)$$

PROOF Property (16) is clear in view of definition (11) and the fact that  $\mathcal{E}_{\mathcal{I}^0}(\phi) \subset \mathcal{E}_{\mathcal{I}}(\phi)$  if  $\mathcal{I} \subset \mathcal{I}^0$ . Now, suppose, in addition, that  $|D\widehat{\phi}_{\mathcal{I}}| > 0$  on  $\mathcal{M}_{\mathcal{I}}(\phi)$  for all  $\mathcal{I} \in \mathbb{I}_k^2$ . Then we have (15) for any  $\ell \in \mathcal{K} \setminus \{k\}$ . If  $\partial\Omega_k(\phi) \cap \mathcal{D} = \emptyset$ , then (17) is trivially satisfied, otherwise take  $x \in \partial\Omega_k(\phi) \cap \mathcal{D}$ . Since  $\partial\Omega_k(\phi) = \overline{\Omega_k(\phi)} \setminus \Omega_k(\phi)$ , it is not possible that  $\phi_k(x) < \phi_\ell(x)$  for all  $\ell \in \mathcal{K} \setminus \{k\}$ , otherwise  $x \in \Omega_k(\phi)$  in view of (4). Thus, we must have  $\phi_k(x) = \phi_\ell(x)$  for some  $\ell \in \mathcal{K} \setminus \{k\}$ . In view of (5) this implies  $x \in \overline{\Omega_\ell(\phi)} \cap \mathcal{D}$ . Then,  $x$  cannot belong to  $\Omega_\ell(\phi)$ , otherwise there would exist an open ball  $B(x, r) \subset \Omega_\ell(\phi)$  with a non-empty intersection with  $\Omega_k(\phi)$  and  $\Omega_k(\phi) \cap \Omega_\ell(\phi)$  would not be empty, which would contradict (15). Thus,  $x \in \partial\Omega_\ell(\phi) \cap \mathcal{D}$  and, in turn,  $x \in \mathcal{E}_{\{k, \ell\}}(\phi)$ , so this proves the other inclusion and yields (17). ■

We now present a simple two-dimensional example to illustrate Lemma 1, Lemma 2 and Lemma 3.

EXAMPLE 1 *Let  $d = 2$ ,  $\mathcal{D} = (0, 1)^2$ ,  $\mathcal{K} = \{0, 1, 2\}$ ,  $\mathcal{I} = \{k_1, k_2\} = \{0, 1\}$ ,  $|\mathcal{I}| = 2$ , and choose  $\phi_0 \equiv 0$ ,  $\phi_1(x_1, x_2) = x_2 - x_1$ ,  $\phi_2(x_1, x_2) = 1 - x_1 - x_2$ . Then we have  $\widehat{\phi}_{\mathcal{I}} = (\widehat{\phi}_1) = (\phi_{k_1} - \phi_{k_2}) = (\phi_0 - \phi_1) = (-\phi_1)$  and*

$$D\widehat{\phi}_{\mathcal{I}}(x) = \begin{pmatrix} 1 & -1 \end{pmatrix}. \quad (18)$$

Clearly,  $D\widehat{\phi}_{\mathcal{I}}(x)$  has rank 1 for any  $x \in \mathcal{D}$ , so we can apply Lemma 2. This shows that  $\mathcal{M}_{\{0,1\}}(\phi)$  is the intersection of a  $\mathcal{C}^\infty$ -manifold of dimension  $d - (|\mathcal{I}| - 1) = 1$  with  $\overline{\mathcal{D}}$ . An explicit calculation using (10) yields

$$\mathcal{M}_{\{0,1\}}(\phi) = \{x \in \overline{\mathcal{D}} \mid \phi_1(x) = 0\} = \{x \in \overline{\mathcal{D}} \mid x_1 = x_2\},$$

so  $\mathcal{M}_{\{0,1\}}(\phi)$  is a diagonal of the square  $\mathcal{D}$ . The sets  $\mathcal{M}_{\{0,2\}}(\phi)$  and  $\mathcal{M}_{\{1,2\}}(\phi)$  can be computed in a similar way.

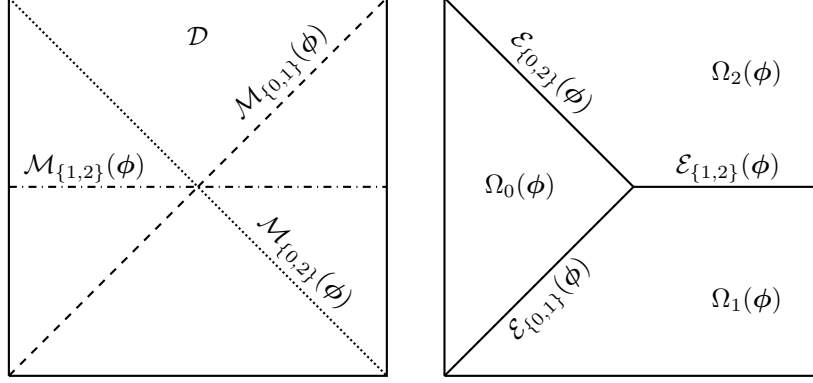


Figure 1: Illustration of the sets  $\mathcal{D} = (0, 1)^2$ ,  $\mathcal{M}_{\mathcal{I}}(\phi)$  (left) and  $\Omega_k(\phi)$ ,  $\mathcal{E}_{\mathcal{I}}(\phi)$  (right) for  $\mathcal{I} = \{0, 1\}, \{0, 2\}, \{1, 2\}$  from Example 1, and of the triple point  $\mathcal{E}_{\{0,1,2\}}(\phi) = \{(\frac{1}{2}, \frac{1}{2})\}$  from Example 2. Note that  $\mathcal{E}_{\mathcal{I}}(\phi) \subsetneq \mathcal{M}_{\mathcal{I}}(\phi)$  for all  $\mathcal{I} = \{0, 1\}, \{0, 2\}, \{1, 2\}$

The lower envelope is  $E_\phi = \phi_1 \chi_{\Omega_1(\phi)} + \phi_2 \chi_{\Omega_2(\phi)}$  with

$$\begin{aligned} \Omega_0(\phi) &= \{x \in \mathcal{D} \mid 0 < \phi_1(x) \text{ and } 0 < \phi_2(x)\} \\ &= \{x \in \mathcal{D} \mid x_1 < x_2 \text{ and } x_2 < 1 - x_1\}, \\ \Omega_1(\phi) &= \{x \in \mathcal{D} \mid \phi_1(x) < 0 \text{ and } \phi_1(x) < \phi_2(x)\} \\ &= \{x \in \mathcal{D} \mid x_2 < x_1 \text{ and } 2x_2 < 1\}, \\ \Omega_2(\phi) &= \{x \in \mathcal{D} \mid \phi_2(x) < 0 \text{ and } \phi_2(x) < \phi_1(x)\} \\ &= \{x \in \mathcal{D} \mid 1 - x_1 < x_2 \text{ and } 1 < 2x_2\}. \end{aligned}$$

Then, we compute

$$\mathcal{E}_{\{0,1\}}(\phi) = \partial\Omega_0(\phi) \cap \partial\Omega_1(\phi) = \{x \in \bar{\mathcal{D}} \mid x_1 = x_2 \text{ and } x_2 \leq 1/2\} \subsetneq \mathcal{M}_{\{0,1\}}(\phi),$$

and we obtain similar characterizations for  $\mathcal{E}_{\{0,2\}}(\phi)$  and  $\mathcal{E}_{\{1,2\}}(\phi)$ ; see Fig. 1 for an illustration of the geometry.

Finally, we can check that  $|D\hat{\phi}_{\mathcal{I}}| > 0$  on  $\mathcal{M}_{\mathcal{I}}(\phi)$  for all  $\mathcal{I} \in \mathbb{I}_0^2$ , thus (17) holds for  $k = 0$ , according to Lemma 3, and (17) becomes in this specific case

$$\mathcal{D} \cap (\mathcal{E}_{\{0,1\}}(\phi) \cup \mathcal{E}_{\{0,2\}}(\phi)) = \mathcal{D} \cap (\mathcal{E}_{\{0,1\}}(\phi) \cup \mathcal{E}_{\{0,2\}}(\phi) \cup \mathcal{E}_{\{0,1,2\}}(\phi)) = \mathcal{D} \cap \partial\Omega_0(\phi);$$

see Fig. 1. Similar properties are obtained for  $k = 1$  and  $k = 2$  in (17) by applying Lemma 3.

In Lemma 2 we have treated the case  $|\mathcal{I}| \leq d$ . Now we treat the degenerate case of  $|\mathcal{I}| \geq d + 1$ , where  $\mathcal{M}_{\mathcal{I}}(\phi)$  has zero dimension.

LEMMA 4 *Assume  $\kappa \geq d + 1$  and  $\mathcal{I} \subset \mathcal{K}$  with  $|\mathcal{I}| \geq d + 1$ , then we have*

$$\mathcal{E}_{\mathcal{I}}(\phi) \subset \mathcal{M}_{\mathcal{I}}(\phi). \quad (19)$$

*Suppose that  $D\widehat{\phi}_{\mathcal{I}}(x)$  has rank  $d$  for all  $x \in \mathcal{M}_{\mathcal{I}}(\phi)$ , then either  $\mathcal{M}_{\mathcal{I}}(\phi) = \emptyset$  or  $\mathcal{M}_{\mathcal{I}}(\phi)$  is a set of isolated points. If, in addition,  $\kappa = d + 1$  and  $\mathcal{I} = \mathcal{K}$ , we also have*

$$\mathcal{E}_{\mathcal{I}}(\phi) = \mathcal{M}_{\mathcal{I}}(\phi). \quad (20)$$

PROOF First of all we can prove that  $\mathcal{E}_{\mathcal{I}}(\phi) \subset \mathcal{M}_{\mathcal{I}}(\phi)$  in a similar way as in the case of Lemma 2. Now, assume  $\mathcal{M}_{\mathcal{I}}(\phi) \neq \emptyset$  and let  $x \in \mathcal{M}_{\mathcal{I}}(\phi)$ . Thanks to the assumption that  $D\widehat{\phi}_{\mathcal{I}}(x)$  has rank  $d$ , there exists a subset  $\mathcal{I}^0 \subset \mathcal{I}$  with cardinal  $|\mathcal{I}^0| = d + 1$  such that the square matrix  $D\widehat{\phi}_{\mathcal{I}^0}(x)$  is invertible. In view of Definition 2 we have  $\mathcal{M}_{\mathcal{I}}(\phi) \subset \mathcal{M}_{\mathcal{I}^0}(\phi)$ , and we also have  $\widehat{\phi}_{\mathcal{I}^0}(x) = 0$ , due to (10). Thus, we can apply the inverse function theorem, and there exists an open ball  $B(x, \delta)$  for some  $\delta > 0$  such that  $(\widehat{\phi}_{\mathcal{I}^0})|_{B(x, \delta)}$  is a diffeomorphism. This yields  $\widehat{\phi}_{\mathcal{I}^0}^{-1}(\{0\}) \cap \mathcal{D} = \{x\}$  and  $\widehat{\phi}_{\mathcal{I}^0}(y) \neq 0$  for  $y \in B(x, \delta) \setminus \{x\}$ , which shows that  $x$  is an isolated zero of  $\widehat{\phi}_{\mathcal{I}^0}$ , hence  $\mathcal{M}_{\mathcal{I}^0}(\phi)$  is a set of isolated points. Since  $\mathcal{M}_{\mathcal{I}}(\phi) \subset \mathcal{M}_{\mathcal{I}^0}(\phi)$ ,  $\mathcal{M}_{\mathcal{I}}(\phi)$  is also a set of isolated points.

Now we consider the particular case of  $\kappa = d + 1$  and  $\mathcal{I} = \mathcal{K}$ . In this case,  $D\widehat{\phi}_{\mathcal{I}}(x)$  is a square matrix and the assumption that  $D\widehat{\phi}_{\mathcal{I}}(x)$  has rank  $d$  is equivalent to  $D\widehat{\phi}_{\mathcal{I}}(x)$  being invertible. Let  $x \in \mathcal{M}_{\mathcal{I}}(\phi)$ , then we have, by definition, that  $\phi_k(x) = \phi_\ell(x)$  for all  $k, \ell \in \mathcal{K}$ . In view of (5), this means that  $x \in \overline{\Omega_k(\phi)}$  for all  $k \in \mathcal{K}$ .

We prove now that  $x \in \partial\Omega_k(\phi)$  for all  $k \in \mathcal{K}$ . Indeed, assume that  $x \in \Omega_k(\phi)$  for some  $k \in \mathcal{K}$ . In this case we prove that  $x \notin \Omega_\ell(\phi)$  for all  $\ell \in \mathcal{K} \setminus \{k\}$ , otherwise there would exist some  $\ell \in \mathcal{K} \setminus \{k\}$  such that  $x \in \Omega_k(\phi) \cap \Omega_\ell(\phi)$ . Since this intersection is open, there would exist  $B(x, r) \subset \Omega_k(\phi) \cap \Omega_\ell(\phi)$  with  $r > 0$ , and we would have  $\phi_k(y) = \phi_\ell(y)$  for all  $y \in B(x, r)$ , due to (5). This would imply that  $D\widehat{\phi}_{\mathcal{I}}(x)$  is not invertible, which leads to a contradiction. Thus, we must have  $x \in \partial\Omega_\ell(\phi)$  for all  $\ell \in \mathcal{K} \setminus \{k\}$ . We can now finish proving that assuming  $x \in \Omega_k(\phi)$  for some  $k \in \mathcal{K}$  leads to a contradiction. Indeed, we would then have  $B(x, r) \subset \Omega_k(\phi)$  and  $B(x, r) \cap \Omega_\ell(\phi) \neq \emptyset$ , for any  $r > 0$  sufficiently small, and, in turn, there would exist  $y \in \Omega_k(\phi) \cap \Omega_\ell(\phi) \cap B(x, r)$  and  $D\widehat{\phi}_{\mathcal{I}}(y)$  would again not be invertible. Choosing  $r$  sufficiently small, and considering that  $\widehat{\phi}_{\mathcal{I}}$  is smooth, this would contradict the hypothesis that  $D\widehat{\phi}_{\mathcal{I}}(x)$  be invertible. Thus, the initial assumption  $x \in \Omega_k(\phi)$  for some  $k \in \mathcal{K}$  is not possible, and this proves that  $x \in \partial\Omega_k(\phi)$  for all  $k \in \mathcal{K}$ . In this way we obtain  $x \in \mathcal{E}_{\mathcal{I}}(\phi)$  and consequently  $\mathcal{M}_{\mathcal{I}}(\phi) \subset \mathcal{E}_{\mathcal{I}}(\phi)$ , which yields (20). ■

DEFINITION 3 *When  $|\mathcal{I}| = d+1$  and the assumptions of Lemma 4 are satisfied, the elements of  $\mathcal{E}_{\mathcal{I}}(\phi)$  are called  $(d+1)$ -tuple points. In the particular case of  $d = 2$ ,  $(d+1)$ -tuple points are called triple points following the standard denomination.*

This means that in the case of  $|\mathcal{I}| = d+1$ , the elements of  $\mathcal{E}_{\mathcal{I}}(\phi)$  belong to the boundary of exactly  $d+1$  phases. The  $(d+1)$ -tuple points play an important role in the LEM, due to their stability with respect to small perturbations of  $\phi$ , see Section 5.2. When  $|\mathcal{I}| > d+1$  and  $\mathcal{E}_{\mathcal{I}}(\phi)$  is not empty, then the points of  $\mathcal{E}_{\mathcal{I}}(\phi)$  belong to the boundary of more than  $d+1$  phases, and one can show that such points are unstable for small perturbations of  $\phi$ , see Example 4 and Section 5.2.

EXAMPLE 2 *Consider the same functions as in Example 1, but now with  $|\mathcal{I}| = d+1 = 3$  and  $\mathcal{I} = \{k_1, k_2, k_3\} = \mathcal{K} = \{0, 1, 2\}$ . We also have*

$$\widehat{\phi}_{\mathcal{I}} = (\widehat{\phi}_1, \widehat{\phi}_2) = (\phi_{k_1} - \phi_{k_2}, \phi_{k_1} - \phi_{k_3}) = (\phi_0 - \phi_1, \phi_0 - \phi_2) = (-\phi_1, -\phi_2)$$

which yields

$$D\widehat{\phi}_{\mathcal{I}}(x) = \begin{pmatrix} -1 & 1 \\ -1 & -1 \end{pmatrix}.$$

Clearly,  $D\widehat{\phi}_{\mathcal{I}}(x)$  is invertible for any  $x \in \mathcal{D}$ , so the assumptions of Lemma 4 are satisfied, yielding  $\mathcal{M}_{\mathcal{I}}(\phi) = \mathcal{E}_{\mathcal{I}}(\phi)$ . Furthermore, it is easy to see that  $\mathcal{M}_{\mathcal{I}}(\phi) = \mathcal{E}_{\mathcal{I}}(\phi) = \{(\frac{1}{2}, \frac{1}{2})\}$  as in (20), see Fig. 1.

EXAMPLE 3 *Let  $d = 3$ ,  $\mathcal{D} = (0, 1)^3$ ,  $\mathcal{K} = \{0, 1, 2, 3\}$ ,  $\mathcal{I} = \{k_1, k_2, k_3\} = \{0, 1, 2\}$ ,  $|\mathcal{I}| = 3$ , and choose  $\phi_0 \equiv 0$ ,  $\phi_1(x_1, x_2, x_3) = x_2 - x_1$ ,  $\phi_2(x_1, x_2, x_3) = 1 - x_1 - x_2$ ,  $\phi_3(x_1, x_2, x_3) = x_3 - 0.5$ . Then we have  $\widehat{\phi}_{\mathcal{I}} = (\widehat{\phi}_1, \widehat{\phi}_2) = (\phi_{k_1} - \phi_{k_2}, \phi_{k_1} - \phi_{k_3}) = (\phi_0 - \phi_1, \phi_0 - \phi_2) = (-\phi_1, -\phi_2)$  and*

$$D\widehat{\phi}_{\mathcal{I}}(x) = \begin{pmatrix} 1 & -1 & 0 \\ 1 & 1 & 0 \end{pmatrix} \quad (21)$$

and  $D\widehat{\phi}_{\mathcal{I}}(x)$  has rank 2 for any  $x \in \mathcal{D}$ . In view of Lemma 2,  $\mathcal{M}_{\mathcal{I}}(\phi)$  is the intersection of a  $\mathcal{C}^\infty$ -manifold of dimension  $d - (|\mathcal{I}| - 1) = 1$  with  $\overline{\mathcal{D}}$ .

Now suppose  $\mathcal{I} = \{k_1, k_2, k_3, k_4\} = \{0, 1, 2, 3\} = \mathcal{K}$ , in this case we have

$$D\widehat{\phi}_{\mathcal{I}}(x) = \begin{pmatrix} 1 & -1 & 0 \\ 1 & 1 & 0 \\ 0 & 0 & -1 \end{pmatrix} \quad (22)$$

which has rank 3 for any  $x \in \mathcal{D}$ , so we conclude, in view of (20), that  $\mathcal{E}_{\mathcal{I}}(\phi) = \mathcal{M}_{\mathcal{I}}(\phi)$  is a set of isolated points. An explicit calculation actually shows that  $\mathcal{M}_{\mathcal{I}}(\phi) = \mathcal{E}_{\mathcal{I}}(\phi) = \{(\frac{1}{2}, \frac{1}{2}, \frac{1}{2})\}$ .

EXAMPLE 4 We present here an example based on a two-dimensional time-dependent Voronoi diagram with four phases, see Birgin, Laurain and Menezes (2023), Example 8. Let  $d = 2$ ,  $\mathcal{D} = (-1, 1)^2$ ,  $\mathcal{K} = \{0, 1, 2, 3\}$ , and choose  $\phi_k(x) = \|x - a_k\|^2$ ,  $k \in \mathcal{K}$ , with  $a_0 = (-1/2 - t, 0)$ ,  $a_1 = (0, -1/2)$ ,  $a_2 = (1/2 + t, 0)$ ,  $a_3 = (0, 1/2)$ , where  $t \geq 0$  is a small parameter. On the one hand we compute, assuming  $t > 0$ ,

$$\mathcal{E}_{\{0,1,2\}}(\phi) = \partial\Omega_0(\phi) \cap \partial\Omega_1(\phi) \cap \partial\Omega_2(\phi) = \emptyset$$

and

$$\mathcal{M}_{\{0,1,2\}}(\phi) = \{x \in \overline{\mathcal{D}} \mid \phi_0(x) = \phi_1(x) = \phi_2(x)\} = \{(0, t + t^2)\}.$$

On the other hand, assuming  $t > 0$ , we have

$$\mathcal{E}_{\{1,2,3\}}(\phi) = \mathcal{M}_{\{1,2,3\}}(\phi) = \left\{ \left( \frac{t + t^2}{1 + 2t}, 0 \right) \right\}.$$

Thus, we have shown, for  $t > 0$ , that  $\mathcal{E}_{\{0,1,2\}}(\phi) \subsetneq \mathcal{M}_{\{0,1,2\}}(\phi)$ , whereas  $\mathcal{E}_{\{1,2,3\}}(\phi) = \mathcal{M}_{\{1,2,3\}}(\phi)$ , which illustrates the results of Lemma 4. In this case,  $\mathcal{E}_{\{1,2,3\}}(\phi)$  is a triple point, see Definition 3. As already discussed above,  $\mathcal{M}_{\{0,1,2\}}(\phi)$  can be seen here as a “ghost” triple point, hidden by the phase  $\Omega_3(\phi)$ .

In the case of  $t = 0$  we have  $\mathcal{E}_{\{0,1,2,3\}}(\phi) = \mathcal{M}_{\{0,1,2,3\}}(\phi) = \{(0, 0)\}$ . This illustrates the case of  $4 = |\mathcal{I}| > d + 1 = 3$  in Lemma 4. Note that in this case,  $\mathcal{E}_{\{0,1,2,3\}}(\phi)$  is on the boundary of the four phases  $\Omega_k(\phi)$ ,  $k \in \mathcal{K}$ . This example shows the instability of such points, in the sense that for  $t > 0$ , this quadruple point immediately splits into two stable triple points  $\left( \pm \frac{t+t^2}{1+2t}, 0 \right)$ , see Fig. 2 and Section 5.2.

Gathering the results of this section, we have obtained a condition on  $\phi$  so that the phases  $\Omega_k(\phi)$ ,  $k \in \mathcal{K}$ , form a partition of  $\mathcal{D}$ , and that the dimension of the boundary of  $\Omega_k(\phi)$  is at most  $d - 1$ , i.e., the boundaries are not “thick”. In fact, we have obtained a stronger result in this section, since we have shown in Lemma 2 that the intersection of the boundaries of  $\Omega_k(\phi)$  for  $k \in \mathcal{I}$  has at most dimension  $d - (|\mathcal{I}| - 1)$ , which allows for avoiding degenerate situations. An example of a degenerate situation occurs when  $\Omega_k(\phi)$ ,  $k \in \mathcal{K} = \{0, 1, 2\}$  are two-dimensional sets, but  $\mathcal{E}_{\{0,1,2\}}(\phi) = \partial\Omega_0(\phi) \cap \partial\Omega_1(\phi) \cap \partial\Omega_2(\phi)$  is a one-dimensional set instead of a zero-dimensional set.

We summarize these results in Theorem 1. We first define partitions of  $\mathcal{D}$ , indexed by  $\mathcal{K}$ .

DEFINITION 4 ( $\mathcal{K}$ -PARTITIONS OF  $\mathcal{D}$ ) Let  $\mathbb{P}$  denote the set of open subsets of  $\mathcal{D} \subset \mathbb{R}^d$ . For  $\mathcal{K} = \{0, 1, \dots, \kappa - 1\} \subset \mathbb{N}$ ,  $\mathbb{P}_{\mathcal{K}}(\mathcal{D})$  denotes the set of vectors of

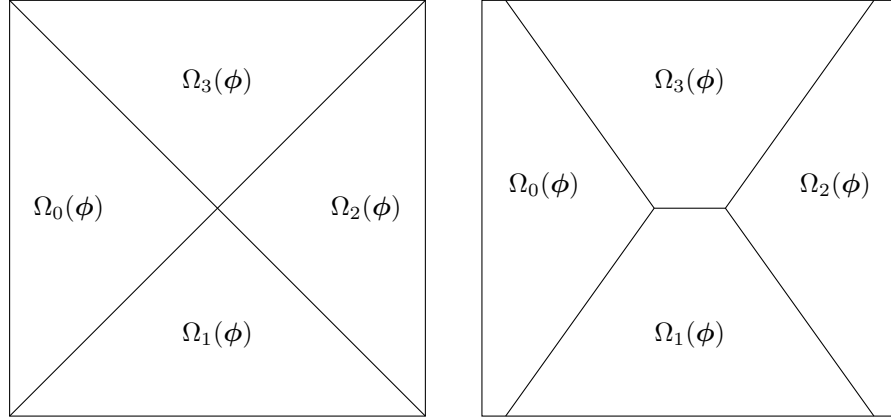


Figure 2: Illustration of Example 4. On the left, the four phases  $\Omega_k(\phi)$ ,  $k \in \mathcal{K} = \{0, 1, 2, 3\}$  at  $t = 0$  with the quadruple point  $\mathcal{E}_{\{0,1,2,3\}}(\phi) = \mathcal{M}_{\{0,1,2,3\}}(\phi) = (0, 0)$  in the center. On the right, the four phases at  $t > 0$ , illustrating how the quadruple point  $(0, 0)$  at  $t = 0$  splits into two stable triple points  $(\pm \frac{t+t^2}{1+2t}, 0)$  at  $t > 0$

domains  $\mathbf{\Omega} := (\Omega_0, \dots, \Omega_{\kappa-1})$  with  $\Omega_k \in \mathbb{P}$  for all  $k \in \mathcal{K}$ ,  $\Omega_k \cap \Omega_\ell = \emptyset$  for all  $\{k, \ell\} \subset \mathcal{K}$ ,  $k \neq \ell$  and  $\bigcup_{k \in \mathcal{K}} \overline{\Omega_k} = \overline{\mathcal{D}}$ .

**THEOREM 1** Let  $\mathcal{K} = \{0, 1, \dots, \kappa - 1\} \subset \mathbb{N}$ ,  $k \in \mathcal{K}$ ,  $\phi \in \mathcal{C}^\infty(\mathbb{R}^d, \mathbb{R}^\kappa)$  and let  $\Omega_k(\phi)$  be defined as in Definition 1. Then, if  $|D\widehat{\phi}_{\mathcal{I}}| > 0$  on  $\mathcal{M}_{\mathcal{I}}(\phi)$  for all  $\mathcal{I} \in \mathbb{I}_k^2$ , we have

$$\mathbf{\Omega}(\phi) := (\Omega_0(\phi), \dots, \Omega_{\kappa-1}(\phi)) \in \mathbb{P}_{\mathcal{K}}(\mathcal{D})$$

and the dimension of  $\partial\Omega_k(\phi)$  is at most  $d - 1$ .

**PROOF** The fact that  $\mathbf{\Omega}(\phi) \in \mathbb{P}_{\mathcal{K}}(\mathcal{D})$  is an immediate consequence of Proposition 1, Lemma 1 and Definition 4. A direct application of Lemma 2 in the case of  $|\mathcal{I}| = 2$  shows that the dimension of  $\partial\Omega_k(\phi)$  is at most  $d - 1$ . ■

### 3. Multiphase shape optimization

We assume that  $\mathcal{D}$  is a Lipschitz, simply connected, and piecewise  $\mathcal{C}^1$  domain. Denote by  $\mathcal{S}$  the set of singular points of  $\partial\mathcal{D}$ , then the outward unit normal

vector  $\mathbf{n}$  to  $\mathcal{D}$  is well-defined on  $\partial\mathcal{D} \setminus \mathcal{S}$ . For  $r \geq 1$  we define

$$\mathcal{C}_c^r(\mathcal{D}, \mathbb{R}^d) := \{\boldsymbol{\theta} \in \mathcal{C}^r(\mathcal{D}, \mathbb{R}^d) \mid \boldsymbol{\theta} \text{ has compact support in } \mathcal{D}\}, \quad (23)$$

$$\mathcal{C}_{\partial\mathcal{D}}^r(\overline{\mathcal{D}}, \mathbb{R}^d) := \{\boldsymbol{\theta} \in \mathcal{C}^r(\overline{\mathcal{D}}, \mathbb{R}^d) \mid \boldsymbol{\theta} \cdot \mathbf{n} = 0 \text{ on } \partial\mathcal{D} \setminus \mathcal{S} \text{ and } \boldsymbol{\theta} = 0 \text{ on } \mathcal{S}\}. \quad (24)$$

Consider a vector field  $\boldsymbol{\theta} \in \mathcal{C}_{\partial\mathcal{D}}^1(\overline{\mathcal{D}}, \mathbb{R}^d)$  and the associated flow  $\Phi_t^\boldsymbol{\theta} : \overline{\mathcal{D}} \rightarrow \overline{\mathcal{D}}$ ,  $t \in [0, t_0]$ , defined for each  $x_0 \in \overline{\mathcal{D}}$  as  $\Phi_t^\boldsymbol{\theta}(x_0) := \mathbf{x}(t)$ , where  $\mathbf{x} : [0, t_0] \rightarrow \mathbb{R}^d$  is the solution to

$$\dot{\mathbf{x}}(t) = \boldsymbol{\theta}(\mathbf{x}(t)) \quad \text{for } t \in [0, t_0], \quad \mathbf{x}(0) = x_0. \quad (25)$$

For  $\Omega \in \mathbb{P}$ , we consider the family of perturbed domains

$$\Omega_t := \Phi_t^\boldsymbol{\theta}(\Omega). \quad (26)$$

In a similar way, for  $\boldsymbol{\Omega} \in \mathbb{P}_{\mathcal{K}}(\mathcal{D})$  we define

$$\boldsymbol{\Omega}_t := \Phi_t^\boldsymbol{\theta}(\boldsymbol{\Omega}) = (\Phi_t^\boldsymbol{\theta}(\Omega_0), \dots, \Phi_t^\boldsymbol{\theta}(\Omega_{\kappa-1})). \quad (27)$$

For  $t_0$  sufficiently small, it can be shown that  $\Phi_t^\boldsymbol{\theta} : \overline{\mathcal{D}} \rightarrow \overline{\mathcal{D}}$  is bijective and for all open sets  $\mathcal{O} \subset \mathcal{D}$ ,  $\Phi_t^\boldsymbol{\theta}$  maps interior points of  $\mathcal{O}$  onto interior points of  $\Phi_t^\boldsymbol{\theta}(\mathcal{O})$  and boundary points of  $\mathcal{O}$  onto boundary points of  $\Phi_t^\boldsymbol{\theta}(\mathcal{O})$ ; see Delfour and Zolésio (2011, Chapter 4, Section 5.1 and Remark 5.2). A similar result holds if we take  $\boldsymbol{\theta} \in \mathcal{C}_c^1(\mathcal{D}, \mathbb{R}^d)$  instead of  $\boldsymbol{\theta} \in \mathcal{C}_{\partial\mathcal{D}}^1(\overline{\mathcal{D}}, \mathbb{R}^d)$ . This implies that  $\boldsymbol{\Omega}_t \in \mathbb{P}_{\mathcal{K}}(\mathcal{D})$  for all  $t \in [0, t_0]$ . When there is no ambiguity, we will often write  $\Phi_t$  for simplicity instead of  $\Phi_t^\boldsymbol{\theta}$  in the rest of the paper.

We are now ready to give the definition of shape differentiability.

**DEFINITION 5 (SHAPE DERIVATIVE)** *Let  $J : \mathbb{P} \rightarrow \mathbb{R}$  be a shape functional.*

- (i) *The Eulerian semiderivative of  $J$  at  $\Omega$  in direction  $\boldsymbol{\theta} \in \mathcal{C}_{\partial\mathcal{D}}^1(\overline{\mathcal{D}}, \mathbb{R}^d)$  is defined by, when the limit exists,*

$$dJ(\Omega)(\boldsymbol{\theta}) := \lim_{t \searrow 0} \frac{J(\Omega_t) - J(\Omega)}{t}. \quad (28)$$

- (ii)  *$J$  is said to be shape differentiable at  $\Omega$  if it has a Eulerian semiderivative at  $\Omega$  for all  $\boldsymbol{\theta} \in \mathcal{C}_{\partial\mathcal{D}}^1(\overline{\mathcal{D}}, \mathbb{R}^d)$  and the mapping*

$$dJ(\Omega) : \mathcal{C}_{\partial\mathcal{D}}^1(\overline{\mathcal{D}}, \mathbb{R}^d) \rightarrow \mathbb{R}, \quad \boldsymbol{\theta} \mapsto dJ(\Omega)(\boldsymbol{\theta})$$

*is linear and continuous, in which case  $dJ(\Omega)(\boldsymbol{\theta})$  is called the shape derivative of  $J$  at  $\Omega$  in direction  $\boldsymbol{\theta} \in \mathcal{C}_{\partial\mathcal{D}}^1(\overline{\mathcal{D}}, \mathbb{R}^d)$ .*

For a multiphase functional  $\mathcal{J} : \mathbb{P}_{\mathcal{K}}(\mathcal{D}) \rightarrow \mathbb{R}$ , we define the Eulerian shape derivative of  $\mathcal{J}$  at  $\Omega \in \mathbb{P}_{\mathcal{K}}(\mathcal{D})$  in a similar way as

$$d\mathcal{J}(\Omega)(\boldsymbol{\theta}) := \lim_{t \searrow 0} \frac{\mathcal{J}(\Omega_t) - \mathcal{J}(\Omega)}{t}. \quad (29)$$

For transformations  $\Phi_t$ , satisfying  $\Phi_t(\Omega) = \Omega$  for all  $t \in [0, t_0]$ , the shape derivative clearly vanishes. When  $\Omega$  is at least  $\mathcal{C}^1$ , this leads to the following structure theorem, proved by Zolésio (1979), see also Delfour and Zolésio (2011), Sokolowski and Zolésio (1992).

**THEOREM 2 (STRUCTURE THEOREM)** *Let  $\Omega \in \mathbb{P}$  be of class  $\mathcal{C}^{r+1}$ ,  $r \geq 0$ . Suppose  $J$  is shape differentiable at  $\Omega$  and  $dJ(\Omega)$  is continuous for the  $\mathcal{C}_{\partial\mathcal{D}}^r(\mathcal{D}, \mathbb{R}^d)$ -topology. Then, there exists a linear and continuous functional  $L : \mathcal{C}^r(\partial\Omega) \rightarrow \mathbb{R}$  such that for all  $\boldsymbol{\theta} \in \mathcal{C}_{\partial\mathcal{D}}^r(\mathcal{D}, \mathbb{R}^d)$ ,*

$$dJ(\Omega)(\boldsymbol{\theta}) = L(\boldsymbol{\theta}|_{\partial\Omega} \cdot \mathbf{n}). \quad (30)$$

**PROOF** See Delfour and Zolésio (2011, pp. 480-481). ■

Despite its usefulness in the case of two phases, Theorem 2 is not relevant in the multiphase context, where usually all the entries  $\Omega_k$  of the vector  $\Omega \in \mathbb{P}_{\mathcal{K}}(\mathcal{D})$  are curvilinear polygons or even less regular, since they form a partition of  $\mathcal{D}$ . In fact, an abstract structure theorem exists in the case of open sets, see Delfour and Zolésio (2011, Theorem 3.6, pp. 479-480), but when the shape derivative can be written as an integral, a more explicit characterization is needed. In Lamboley and Pierre (2007, Theorem 1.3), a general structure theorem is proven, which shows that the shape derivative can be written as  $L(\boldsymbol{\theta}|_{\partial\Omega} \cdot \mathbf{n})$  even when  $\Omega$  is only a set of finite perimeter, which is, in particular, valid for Lipschitz domains. However, the linear form  $L$  is in general not a boundary integral if  $\Omega$  is only Lipschitz or piecewise  $\mathcal{C}^r$ . For example, the shape derivative of the perimeter contains Dirac measures at the vertices of  $\partial\Omega$  when  $\Omega$  is a polygon; see Lamboley and Pierre (2007, Proposition 2.6).

The structure (30) can be seen as a *strong form* of the shape derivative, in the sense that it requires a strong regularity of the domain, while it tolerates a low regularity of the vector field  $\boldsymbol{\theta}$ . In the multiphase context, it is natural to use weaker structures of the shape derivatives, which are valid for domains with low regularity, but involve the derivatives of  $\boldsymbol{\theta}$  in return, which requires more regularity for  $\boldsymbol{\theta}$ . In the case, where the functional is defined as a volume integral, its shape derivative can be written as a volume integral, instead of a boundary integral, and then we call it *distributed shape derivative*, see (31). Also, it is sometimes possible to write shape derivatives as boundary integrals on Lipschitz domains as in (34). In this case, the structure is slightly weaker than (30), as the linear form depends on  $\boldsymbol{\theta}|_{\partial\Omega}$  instead of  $\boldsymbol{\theta}|_{\partial\Omega} \cdot \mathbf{n}$ . These weaker

expressions, in particular the distributed shape derivative, are key ingredients of the LEM. We discuss now some fundamental properties of weak expressions of shape derivatives. First of all, it is useful to write the distributed shape derivative using a tensor representation (Laurain, 2020; Laurain and Sturm, 2016), as will be seen in Proposition 2.

**DEFINITION 6 (TENSOR REPRESENTATION OF DISTRIBUTED SHAPE DERIVATIVE)** *Let  $\Omega \in \mathbb{P}_{\mathcal{K}}(\mathcal{D})$  and assume that  $\mathcal{J} : \mathbb{P}_{\mathcal{K}}(\mathcal{D}) \mapsto \mathbb{R}$  has a shape derivative at  $\Omega$ . The shape derivative of  $\mathcal{J}$  admits a tensor representation of order 1 if there exist a first-order tensor  $\mathbf{S}_0 \in L^1(\mathcal{D}, \mathbb{R}^d)$  and a second order tensor  $S_1 \in L^1(\mathcal{D}, \mathbb{R}^{d \times d})$  such that for all  $\theta \in \mathcal{C}_{\partial \mathcal{D}}^1(\overline{\mathcal{D}}, \mathbb{R}^d)$ ,*

$$d\mathcal{J}(\Omega)(\theta) = \int_{\mathcal{D}} S_1 : D\theta + \mathbf{S}_0 \cdot \theta. \quad (31)$$

The following proposition extends the result of Laurain and Sturm (2016, Proposition 4.3) to the multiphase case, also requiring weaker regularity assumptions.

**PROPOSITION 2** *Assume  $\Omega \in \mathbb{P}_{\mathcal{K}}(\mathcal{D})$ ,  $\theta \in \mathcal{C}_{\partial \mathcal{D}}^1(\overline{\mathcal{D}}, \mathbb{R}^d)$ , and that  $\mathcal{J}$  has an Eulerian shape derivative at  $\Omega$  with the tensor representation (31). If  $S_1 \in W^{1,1}(\Omega_k, \mathbb{R}^{d \times d})$  for all  $k \in \mathcal{K}$ , then*

$$\operatorname{div}(S_1) = \mathbf{S}_0 \quad \text{in } \Omega_k \text{ for all } k \in \mathcal{K}, \quad (32)$$

where  $\operatorname{div}(S_1)$  is defined as the vector of the divergence of the rows of  $S_1$ , and

$$d\mathcal{J}(\Omega)(\theta) = \sum_{k \in \mathcal{K}} \int_{\Omega_k} \operatorname{div}(S_1^T \theta). \quad (33)$$

If, in addition,  $\Omega_k$  is Lipschitz for all  $k \in \mathcal{K}$ , then we have the boundary expression

$$d\mathcal{J}(\Omega)(\theta) = \sum_{k \in \mathcal{K}} \int_{\partial \Omega_k} (S_{1,k} \mathbf{n}_k) \cdot \theta, \quad (34)$$

where  $S_{1,k}$  is the trace on  $\partial \Omega_k$  of  $S_1|_{\Omega_k}$  and  $\mathbf{n}_k$  is the outward unit normal vector to  $\Omega_k$ .

**PROOF** The proof is a straightforward adaptation to the multiphase context of the proof of Laurain (2019), Proposition 1.  $\blacksquare$

#### 4. The lower envelope method

In this section the notation  $\phi = (\phi_0, \phi_1, \dots, \phi_{\kappa-1})$  stands for a vector of time-dependent functions  $\phi_k \in \mathcal{C}^\infty([0, t_0] \times \mathbb{R}^d, \mathbb{R})$ . For simplicity, we will sometimes

use the notation  $\phi_k(t) := \phi_k(t, \cdot)$  and  $\phi(t) = (\phi_0(t), \phi_1(t), \dots, \phi_{\kappa-1}(t))$ . The time-dependent phases  $\Omega_k(\phi(t))$ ,  $k \in \mathcal{K}$ , are defined as in (2), and the interfaces  $\mathcal{E}_{\mathcal{I}}(\phi(t))$ ,  $\mathcal{M}_{\mathcal{I}}(\phi(t))$  and  $\widehat{\phi}_{\mathcal{I}}(t)$  as in Definition 2.

#### 4.1. Interface tracking using the lower envelope approach

In this Subsection we give an informal explanation of how the equations for the lower envelope method are derived and how they allow us to track the motion of interfaces in a multiphase setting. The proper definition of the lower envelope method is given in Section 4.4, and its properties are investigated in Section 5.

For  $t \in [0, t_0]$  and  $k \in \mathcal{K}$ , let  $\mathbf{x}(t) \in \partial\Omega_k(\phi(t)) \cap \mathcal{D}$  be a moving interface point. Suppose that for all  $t \in [0, t_0]$ ,  $|D\widehat{\phi}_{\mathcal{I}}(t)| > 0$  on  $\mathcal{M}_{\mathcal{I}}(\phi(t))$  for all  $\mathcal{I} \in \mathbb{I}_k^2$ . Then, for each  $t \in [0, t_0]$ , we can apply Lemma 3, which yields that  $\mathbf{x}(t) \in \mathcal{E}_{\mathcal{I}}(\phi(t))$  for some  $\mathcal{I} \in \mathbb{I}_k^r$  with  $2 \leq r \leq \kappa$ . It can be shown that one can choose  $\mathcal{I}$  independent of  $t$ , using the assumption  $|D\widehat{\phi}_{\mathcal{I}}(t)| > 0$  on  $\mathcal{M}_{\mathcal{I}}(\phi(t))$  for all  $\mathcal{I} \in \mathbb{I}_k^2$  and by taking  $t_0$  sufficiently small; we refer to the perturbation theory for sets defined as intersections, presented in Birgin, Laurain and Menezes (2023, Section 2) for a proof of this type of property in a similar context.

We also suppose that the trajectory of  $\mathbf{x}(t)$  can be described by a flow of the type (25) for some  $\boldsymbol{\theta} \in \mathcal{C}_{\partial\mathcal{D}}^1(\mathcal{D}, \mathbb{R}^d)$ . In view of (12) and (19) we have  $\mathcal{E}_{\mathcal{I}}(\phi(t)) \subset \mathcal{M}_{\mathcal{I}}(\phi(t))$ , consequently,  $\mathbf{x}(t)$  satisfies the  $|\mathcal{I}| - 1$  equations

$$\phi_k(t, \mathbf{x}(t)) = \phi_\ell(t, \mathbf{x}(t)), \quad \text{for all } \ell \in \mathcal{I} \setminus \{k\}. \quad (35)$$

Differentiation of each of these relations with respect to  $t$  yields for  $t \in [0, t_0]$ :

$$\partial_t(\phi_k - \phi_\ell)(t, \mathbf{x}(t)) + \boldsymbol{\theta}(\mathbf{x}(t)) \cdot \nabla(\phi_k - \phi_\ell)(t, \mathbf{x}(t)) = 0, \quad \text{for all } \ell \in \mathcal{I} \setminus \{k\}. \quad (36)$$

We extend equations (36) to  $\mathcal{D}$ , this yields

$$\partial_t(\phi_k - \phi_\ell)(t, x) + \boldsymbol{\theta}(x) \cdot \nabla(\phi_k - \phi_\ell)(t, x) = 0, \quad \text{for all } \ell \in \mathcal{I} \setminus \{k\}, \quad (37)$$

for  $t \in [0, t_0]$  and  $x \in \mathcal{D}$ .

Now, assume that there exists  $\boldsymbol{\psi} \in \mathcal{C}^\infty([0, t_0] \times \mathbb{R}^d, \mathbb{R}^\kappa)$ , solution of

$$\partial_t \psi_k(t, x) + \boldsymbol{\theta}(x) \cdot \nabla \psi_k(t, x) = 0, \quad \text{for all } k \in \mathcal{K}, t \in [0, t_0] \text{ and } x \in \mathcal{D}, \quad (38)$$

$$\psi_k(0, x) = \phi_k(0, x), \quad (39)$$

where  $\psi_k$  are the entries of  $\boldsymbol{\psi}$ . Then, for any  $\mathcal{I} \in \mathbb{I}_k^r$  with  $2 \leq r \leq \kappa$ , we have in view of (38) that  $\psi_k - \psi_\ell$  satisfies (37) for all  $\ell \in \mathcal{I} \setminus \{k\}$ . Since equations (37) are obtained by differentiating the constitutive equations (35), the phases  $\Omega_k(\boldsymbol{\psi}(t))$  represent a first-order approximation of  $\Omega_k(\phi(t))$  for all  $k \in \mathcal{K}$  and

$t \in [0, t_0]$ , for small  $t_0$ . In this sense, it is meaningful to employ the transport equations (38)-(39) as the foundation of the LEM, described in Section 4.4.

In view of Lemma 3,  $\partial\Omega_k(\phi(t))$  is the union of all the sets  $\mathcal{E}_{\mathcal{I}}(\phi(t))$  with  $\mathcal{I} \in \mathbb{I}_k^2$ . In practice, it is common that these sets are non-empty, see Examples 1, 2, 3 and Fig. 1. If this is the case, then in order to describe the evolution of  $\partial\Omega_k(\phi(t))$  we need to solve equations (37) at least for all  $\mathcal{I} \in \mathbb{I}_k^2$ . Thus, in general, we need to solve (37) for all  $\ell \in \mathcal{K} \setminus \{k\}$ , i.e., for  $\kappa - 1$  equations. Note that (38)-(39) actually consists of  $\kappa$  equations, but, in practice, we can take  $\psi_0 \equiv 0$  without loss of generality of the method, so in fact (38)-(39) can be reduced to  $\kappa - 1$  equations. This shows that solving the transport equations (38)-(39) for all  $k \in \mathcal{K}$  is de facto a natural way of tracking the motion of interface points using the lower envelope representation of multiphases.

#### 4.2. On reducing the dimension of velocity fields

An interesting question that naturally arises is to determine whether one needs to use the full vector field  $\boldsymbol{\theta}$  in (38), or if the components of  $\boldsymbol{\theta}$  that are orthogonal to  $\nabla\psi_k$  are superfluous. For instance, in the level set method of Osher and Sethian (1988), which can be seen as a special case of the LEM for two phases (see Section 4.5), one uses only the normal component of  $\boldsymbol{\theta}$ , since the gradient of the level set function is orthogonal to the tangential component of  $\boldsymbol{\theta}$ , in the case of smooth domains. In the multiphase context, however, the situation is more complicated, due to the nonsmoothness of the sets  $\Omega_k(\phi)$ .

We now discuss this issue in more detail. Suppose that the assumptions of either Lemma 2 or Lemma 4 are satisfied for each  $t \in [0, t_0]$ , then we have  $\dim(\mathcal{E}_{\mathcal{I}}(\phi(t))) \leq \max\{d - (|\mathcal{I}| - 1), 0\}$  for all  $\mathcal{I} \subset \mathcal{K}$  with  $|\mathcal{I}| \geq 2$ . Assume, for simplicity, that  $\dim(\mathcal{E}_{\mathcal{I}}(\phi(t))) = \max\{d - (|\mathcal{I}| - 1), 0\}$ . Observe that in this case the codimension of  $\mathcal{E}_{\mathcal{I}}(\phi(t))$  with respect to the ambient space  $\mathbb{R}^d$  is equal to  $\min\{|\mathcal{I}| - 1, d\}$ , and consider the decomposition

$$\boldsymbol{\theta}(\mathbf{x}(t)) = \boldsymbol{\theta}_{\tau}(\mathbf{x}(t)) + \boldsymbol{\theta}_{\perp}(\mathbf{x}(t)),$$

with  $\boldsymbol{\theta}_{\tau}(\mathbf{x}(t)) \in T_{\mathbf{x}(t)}\mathcal{E}_{\mathcal{I}}(\phi(t))$  and  $\boldsymbol{\theta}_{\perp}(\mathbf{x}(t)) \in (T_{\mathbf{x}(t)}\mathcal{E}_{\mathcal{I}}(\phi(t)))^{\perp}$ , where  $T_{\mathbf{x}(t)}\mathcal{E}_{\mathcal{I}}(\phi(t))$  is the tangent space of  $\mathcal{E}_{\mathcal{I}}(\phi(t))$  at  $\mathbf{x}(t) \in \mathcal{E}_{\mathcal{I}}(\phi(t))$  of dimension  $\max\{d - (|\mathcal{I}| - 1), 0\}$ , and  $(T_{\mathbf{x}(t)}\mathcal{E}_{\mathcal{I}}(\phi(t)))^{\perp}$  is its orthogonal complement in  $\mathbb{R}^d$ , of dimension  $\min\{|\mathcal{I}| - 1, d\}$ . Then, for  $k \in \mathcal{I}$ , in view of (35), one observes that  $\nabla(\phi_k - \phi_{\ell})(t, \mathbf{x}(t)) \in (T_{\mathbf{x}(t)}\mathcal{E}_{\mathcal{I}}(\phi(t)))^{\perp}$  for all  $\ell \in \mathcal{I} \setminus \{k\}$ , and consequently, equations (36) become

$$\partial_t(\phi_k - \phi_{\ell})(t, \mathbf{x}(t)) + \boldsymbol{\theta}_{\perp}(\mathbf{x}(t)) \cdot \nabla(\phi_k - \phi_{\ell})(t, \mathbf{x}(t)) = 0, \quad \text{for all } \ell \in \mathcal{I} \setminus \{k\}. \quad (40)$$

In the particular case of  $\mathcal{I} = \mathcal{K} = \{0, 1\}$  and  $\phi_0 \equiv 0$ , which corresponds to the LSM, we have  $\boldsymbol{\theta}_{\perp} = (\boldsymbol{\theta} \cdot \mathbf{n})\mathbf{n}$ , where  $\mathbf{n}$  is the outward unit normal vector

to  $\Omega_0(\phi)$ . This corresponds to the standard simplification made in the LSM, which yields the level set equation; see Sethian (1999).

We may also relate this observation to the structure theorem, Sturm (2016, Corollary 5.6), where it is proven that the shape derivative of functionals taking smooth manifolds of dimension  $d_0$  in  $\mathbb{R}^d$  as argument only depends on the component  $\boldsymbol{\theta}_\perp$  of dimension  $d - d_0$ . Taking  $d_0 = d - (|\mathcal{I}| - 1)$ , we arrive at the same conclusion, i.e., that it is sufficient to use  $\boldsymbol{\theta}_\perp$  to track the motion of  $\mathcal{E}_\mathcal{I}(\phi(t))$ , as in (40).

We observe, however, that the dimension of  $(T_{\mathbf{x}(t)}\mathcal{E}_\mathcal{I}(\phi(t)))^\perp$  depends on  $\mathcal{I}$ , and that in view of Lemma 3,  $\partial\Omega_k(\phi(t))$  is typically the union of sets  $\mathcal{E}_\mathcal{I}(\phi(t))$ , whose dimensions take all integer values between 0 and  $d - 1$ . In particular, when  $|\mathcal{I}| \geq d + 1$ , then Lemma 4 indicates that  $\mathcal{E}_\mathcal{I}(\phi(t))$  is a set of isolated points and  $\dim(T_{\mathbf{x}(t)}\mathcal{E}_\mathcal{I}(\phi(t)))^\perp = \min\{|\mathcal{I}| - 1, d\} = d$ , so that  $\boldsymbol{\theta}_\perp = \boldsymbol{\theta}$  has dimension  $d$ .

In this case, one is constrained to use the full vector  $\boldsymbol{\theta}$  to describe the evolution of  $\partial\Omega_k(\phi(t))$ , at least locally around the sets  $\mathcal{E}_\mathcal{I}(\phi(t))$  with zero dimension. This shows that the lowest-dimensional subsets  $\mathcal{E}_\mathcal{I}(\phi(t))$  of  $\partial\Omega_k(\phi(t))$  dictate the dimension of the vector field  $\boldsymbol{\theta}_\perp$  that should be used to track the motion of  $\partial\Omega_k(\phi(t))$ . From the point of view of numerical implementation, this is in accordance with the use of weak forms of shape derivatives, such as (31) or (34), where the full vector  $\boldsymbol{\theta}$  is naturally available rather than  $\boldsymbol{\theta}_\perp$ . This is a generalization of the idea used in Laurain and Sturm (2016), where the full vector  $\boldsymbol{\theta}$  was used in a distributed shape derivative-based level set method, instead of the normal component  $\boldsymbol{\theta} \cdot \boldsymbol{n}$ , used in the LSM.

### 4.3. Narrow band approach

In the LSM, the level set equations can be solved in a small neighbourhood of the interface to decrease the computational cost; this is the so-called *narrow band* approach. In the case of the lower envelope method, one could also use the same idea and solve equations (38)-(39) in a small neighbourhood of the union of all interfaces  $\cup_{\mathcal{I} \in \mathbb{I}_2^r, r \geq 2} \mathcal{E}_\mathcal{I}(\phi(t))$ .

### 4.4. Description of the lower envelope method

In the previous sections we have provided the theoretical foundation, enabling us to now define the LEM. Given  $\phi_0 \in \mathcal{C}^\infty(\mathbb{R}^d, \mathbb{R}^\kappa)$  an initial vector-valued function, a vector field  $\boldsymbol{\theta} \in \mathcal{C}_{\partial\mathcal{D}}^1(\overline{\mathcal{D}}, \mathbb{R}^d)$  and the associated flow  $\Phi_t^\theta : \overline{\mathcal{D}} \rightarrow \mathbb{R}^d$ , find  $\phi \in \mathcal{C}^\infty([0, t_0] \times \mathbb{R}^d, \mathbb{R}^\kappa)$ , being the solution of the transport equations

$$\partial_t \phi_k(t, x) + \boldsymbol{\theta}(x) \cdot \nabla \phi_k(t, x) = 0, \quad \text{for } t \in [0, t_0] \text{ and } x \in \mathcal{D}, \quad (41)$$

$$\phi_k(0, x) = \phi_{k,0}(x), \quad (42)$$

for all  $k \in \mathcal{K}$ , where  $\phi_k, \phi_{k,0}$  are the entries of  $\phi, \phi_0$ , respectively. The moving vector domain is defined as  $\mathbf{\Omega}_t := (\Omega_0(\phi(t)), \dots, \Omega_{\kappa-1}(\phi(t)))$ , where  $\Omega_k(\phi(t))$  is defined as in (2). Note that we can write (41)-(42) in an equivalent way in vectorial form as

$$\partial_t \phi(t, x) + D\phi(t, x)\boldsymbol{\theta}(x) = 0, \quad \text{for } t \in [0, t_0] \text{ and } x \in \mathcal{D}, \quad (43)$$

$$\phi(0, x) = \phi_0(x). \quad (44)$$

By analogy with the LSM, we call (43)-(44) the *lower envelope equation*. If we assume that for all  $t \in [0, t_0]$  we have  $|D\hat{\phi}_{\mathcal{I}}(t)| > 0$  on  $\mathcal{M}_{\mathcal{I}}(\phi(t))$  for all  $\mathcal{I} \in \mathbb{I}_k^2$ , then this guarantees that  $\mathbf{\Omega}_t \in \mathbb{P}_{\mathcal{K}}(\mathcal{D})$  for all  $t \in [0, t_0]$  in view of Theorem 1.

In a practical implementation, we may choose  $\phi_{0,0} \equiv 0$ , which yields  $\phi_0(t) \equiv 0$  for all  $t \in [0, t_0]$ . This does not reduce the generality of the method and is less expensive from the computational point of view. For shape optimization problems,  $\boldsymbol{\theta}$  is usually chosen as a descent direction for the multiphase cost functional  $\mathcal{J} : \mathbb{P}_{\mathcal{K}}(\mathcal{D}) \rightarrow \mathbb{R}$ , which can be obtained by solving an elliptic PDE using a weak form of the shape derivative on the right-hand side; see Section 6.3 for more details on the procedure.

Note that from a numerical perspective, it is reasonable to work with a time-independent  $\boldsymbol{\theta}$  when solving (43)-(44) over a sufficiently short time interval  $[0, t_0]$  at each iteration of the optimization method. However, to model the evolution of  $\phi$  over a longer time interval, one would need to consider a time-dependent  $\boldsymbol{\theta}$ . This “freezing” of  $\boldsymbol{\theta}$  is performed similarly in the level set method; see Osher and Fedkiw (2003), Osher and Sethian (1988), Sethian (1999).

#### 4.5. The particular case of two phases

In the case of  $\mathcal{K} = \{0, 1\}$ ,  $\phi_1 \in \mathcal{C}^\infty([0, t_0] \times \mathbb{R}^d, \mathbb{R})$  and  $\phi_0 \equiv 0$ , we show that the LEM coincides with the LSM (Osher and Fedkiw, 2003; Osher and Sethian, 1988; Sethian, 1990). First of all, assuming that 0 is a regular value of  $\phi_1(t, \cdot)$  for all  $t \in [0, t_0]$ , Definition 1 yields

$$\Omega_1(\phi(t)) := \{x \in \mathcal{D} \mid \phi_1(t, x) < 0\}, \quad \Omega_0(\phi(t)) := \{x \in \mathcal{D} \mid \phi_1(t, x) > 0\},$$

which corresponds to the definition of the domains in the level set method.

Then, the lower envelope equation (43) reduces to the following transport equation

$$\partial_t \phi_1(t, x) + \boldsymbol{\theta}(x) \cdot \nabla \phi_1(t, x) = 0, \quad \text{for } t \in [0, t_0] \text{ and } x \in \mathcal{D}. \quad (45)$$

Since we have assumed that 0 is a regular value of  $\phi_1(t, \cdot)$  for all  $t \in [0, t_0]$ , then  $\Omega_1(\phi(t))$  is smooth and (45) reduces to the usual level set equation

$$\partial_t \phi_1(t, x) + \boldsymbol{\theta}(x) \cdot \mathbf{n}(x) |\nabla \phi_1(t, x)| = 0, \quad \text{for } t \in [0, t_0] \text{ and } x \in \mathcal{D}. \quad (46)$$

This shows that the LSM is indeed a particular case of the LEM, using two phases.

## 5. Geometric properties of the LEM

### 5.1. Properties of triple points in two dimensions

In this subsection we consider a time-independent setting. We assume  $d = 2$ ,  $\mathcal{K} = \{0, 1, 2\}$ ,  $\boldsymbol{\phi} = (\phi_0, \phi_1, \phi_2) \in \mathcal{C}^\infty(\mathbb{R}^2, \mathbb{R}^3)$ , and  $\phi_0 \equiv 0$ . We also suppose that either the assumptions of Lemma 2, if  $|\mathcal{I}| \leq 2$ , or the assumptions of Lemma 4, if  $|\mathcal{I}| \geq 3$ , are satisfied. Assume that  $\mathcal{E}_{\mathcal{K}}(\boldsymbol{\phi})$  and  $\mathcal{E}_{\{0,1\}}(\boldsymbol{\phi})$ ,  $\mathcal{E}_{\{1,2\}}(\boldsymbol{\phi})$  and  $\mathcal{E}_{\{0,2\}}(\boldsymbol{\phi})$  are not empty. Then,  $\mathcal{E}_{\{0,1\}}(\boldsymbol{\phi})$ ,  $\mathcal{E}_{\{1,2\}}(\boldsymbol{\phi})$  and  $\mathcal{E}_{\{0,2\}}(\boldsymbol{\phi})$  are one-dimensional, according to Lemma 2. Here,  $\mathcal{E}_{\mathcal{K}}(\boldsymbol{\phi})$  is a set of triple points, according to Lemma 4 and Definition 3. Let  $\hat{x} \in \mathcal{E}_{\mathcal{K}}(\boldsymbol{\phi})$  be a triple point. Denote by  $\mathbb{D}_{\mathcal{I}}$  the half-tangent to  $\mathcal{E}_{\mathcal{I}}(\boldsymbol{\phi})$  at  $\hat{x}$  for  $\mathcal{I} = \{0, 1\}$ ,  $\mathcal{I} = \{1, 2\}$  or  $\mathcal{I} = \{0, 2\}$ . Denote by  $\vartheta \in [0, 2\pi]$  the angle in local polar coordinates with origin  $\hat{x}$  and such that  $\vartheta = 0$  corresponds to  $\mathbb{D}_{\{0,2\}}$ . Without loss of generality, we may assume that  $\vartheta_0 \leq \vartheta_1$ , where  $\vartheta_0$  is the angle between  $\mathbb{D}_{\{0,2\}}$  and  $\mathbb{D}_{\{0,1\}}$ , and  $\vartheta_1$  is the angle between  $\mathbb{D}_{\{0,2\}}$  and  $\mathbb{D}_{\{1,2\}}$ . Indeed, if  $\vartheta_0 > \vartheta_1$  we can just exchange the indices of  $\phi_0$  and  $\phi_2$ , rename the phases accordingly, and we will get  $\vartheta_0 \leq \vartheta_1$ . Introduce also the relative angles  $\beta_0 = \vartheta_0 \geq 0$ ,  $\beta_1 = \vartheta_1 - \vartheta_0 \geq 0$  and  $\beta_2 = 2\pi - \vartheta_1 \geq 0$ . Clearly, we have  $\beta_0 + \beta_1 + \beta_2 = 2\pi$ ; see Fig. 3 for an illustration of the geometry.

**THEOREM 3** *Suppose that either the assumptions of Lemma 2, if  $|\mathcal{I}| \leq 2$ , or the assumptions of Lemma 4, if  $|\mathcal{I}| \geq 3$ , are satisfied and the geometry is defined as above. Assume that  $D\hat{\boldsymbol{\phi}}_{\mathcal{K}}(\hat{x})$  is invertible, then*

$$\max_{k \in \mathcal{K}} \beta_k < \pi \text{ and } \min_{k \in \mathcal{K}} \beta_k > 0.$$

**PROOF** First we assume that  $\beta_0 > \pi$  and show that this leads to a contradiction. Without loss of generality we may assume that  $\mathbb{D}_{\{0,2\}}$  coincides with the right semi-axis  $Ox$ . Since  $\beta_0 > \pi$ ,  $\mathbb{D}_{\{0,1\}}$  and  $\mathbb{D}_{\{1,2\}}$  must be both located in the open lower half-plane.

Denote by  $\mathbb{H}_r := \{(x, y) \in \mathbb{R}^2 \mid x > 0\}$  the right open half-plane and  $\mathbb{H}_l := \{(x, y) \in \mathbb{R}^2 \mid x < 0\}$  the left open half-plane. For  $x \in \mathcal{E}_{\{0,2\}}(\boldsymbol{\phi})$  we have  $\nabla_{\Gamma} \phi_2(x) = 0$ , since  $\phi_2 = \phi_0$  on  $\mathcal{E}_{\{0,2\}}(\boldsymbol{\phi})$  and  $\phi_0 \equiv 0$ , where  $\nabla_{\Gamma}$  denotes the tangential gradient on  $\mathcal{E}_{\{0,2\}}(\boldsymbol{\phi})$ . We also have  $\nabla \phi_2(x) \cdot \mathbf{n}_2(x) > 0$  for all  $x \in \mathcal{E}_{\{0,2\}}(\boldsymbol{\phi})$ , where  $\mathbf{n}_2$  is the unit outward normal vector to  $\Omega_2(\boldsymbol{\phi})$ , since

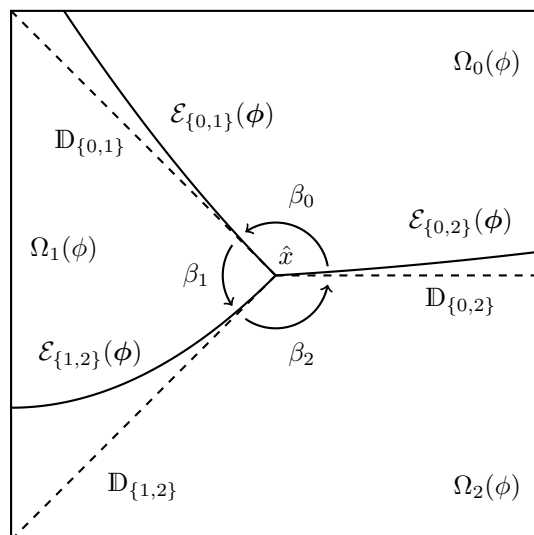


Figure 3: The sets  $\mathcal{D} = (0,1)^2$  and  $\mathcal{E}_{\mathcal{I}}(\phi)$ , half-tangents  $\mathbb{D}_{\mathcal{I}}$  for  $\mathcal{I} = \{0, 1\}, \{0, 2\}, \{1, 2\}$  and angles  $\beta_0, \beta_1, \beta_2$

$\phi_2 \leq \phi_0$  in  $\Omega_2(\phi)$  and  $\phi_2 \geq \phi_0$  in  $\Omega_0(\phi)$ . As  $\mathbb{D}_{\{0,2\}}$  coincides with the right semiaxis  $Ox$ , we get  $\nabla\phi_2(\hat{x}) = (0, \lambda)$  with  $\lambda > 0$ . In a similar way, we have that  $\nabla\phi_1(\hat{x})$  is orthogonal to  $\mathbb{D}_{\{0,1\}}$ , hence  $-\nabla\phi_1(\hat{x}) \in \mathbb{H}_r$ , using the assumption  $\beta_0 > \pi$  and the fact that  $\nabla\phi_1(\hat{x}) \neq 0$ , thanks to the assumption that  $D\hat{\phi}_{\mathcal{K}}(\hat{x})$  is invertible. Thus, we have shown that  $\nabla(\phi_2 - \phi_1)(\hat{x}) \in \mathbb{H}_r$ .

In a similar way we have that  $\nabla(\phi_2 - \phi_1)(\hat{x})$  is orthogonal to  $\mathbb{D}_{\{1,2\}}$ . The fact that  $\phi_2 - \phi_1 \geq 0$  in  $\Omega_1$  and  $\phi_2 - \phi_1 \leq 0$  in  $\Omega_2$  shows that  $\nabla(\phi_2 - \phi_1)(\hat{x})$  is pointing outward from  $\Omega_2$ , therefore it must be in  $\mathbb{H}_l$ , considering the assumption  $\beta_0 > \pi$ . Thus, we have obtained  $\nabla(\phi_2 - \phi_1)(\hat{x}) \in \mathbb{H}_r \cap \mathbb{H}_l$  which is a contradiction, since  $\mathbb{H}_r \cap \mathbb{H}_l = \emptyset$ , and this implies that  $\beta_0 \leq \pi$ . In a similar way, one also proves that  $\beta_k \leq \pi$  for  $k = 1, 2$ .

Now, assume that  $\beta_0 = \pi$ , then  $\nabla\phi_2(\hat{x})$  and  $\nabla\phi_1(\hat{x})$  are linearly dependent, which implies  $\det D\hat{\phi}_{\mathcal{K}}(\hat{x}) = 0$ , and this contradicts the assumption that  $D\hat{\phi}_{\mathcal{K}}(\hat{x})$  be invertible. Hence, we must have  $\beta_0 < \pi$  and also  $\beta_1 < \pi, \beta_2 < \pi$  in a similar way. Then, the fact that  $\min_{k \in \mathcal{K}} \beta_k > 0$  is a straightforward consequence of  $\beta_0 + \beta_1 + \beta_2 = 2\pi$ . ■

We can also compute the angles at the triple point  $\hat{x}$  in the way shown here, as follows:

PROPOSITION 3 *Let  $\hat{x} \in \mathcal{E}_{\mathcal{K}}(\phi)$  and assume  $D\hat{\phi}_{\mathcal{K}}(\hat{x})$  is invertible, then*

$$\beta_k = \arccos \frac{\nabla(\phi_{[k+1]_3} - \phi_k) \cdot \nabla(\phi_k - \phi_{[k+2]_3})}{|\nabla(\phi_{[k+1]_3} - \phi_k)| \cdot |\nabla(\phi_k - \phi_{[k+2]_3})|} \quad \text{for all } k \in \mathcal{K}, \quad (47)$$

where  $[k+1]_3$  means  $k+1$  modulo 3.

PROOF The vector  $\nabla(\phi_2 - \phi_1)$  is orthogonal to  $\mathbb{D}_{\{1,2\}}$  and points outward from  $\Omega_2(\phi)$ , while the vector  $\nabla(\phi_1 - \phi_0)$  is orthogonal to  $\mathbb{D}_{\{0,1\}}$  and points outward from  $\Omega_1(\phi)$ . Hence,  $\beta_1$  is also the angle between  $\nabla(\phi_2 - \phi_1)$  and  $\nabla(\phi_1 - \phi_0)$ , and since  $0 < \beta_1 < \pi$ , according to Theorem 3, this yields (47) for  $k = 1$ . The other cases are established in the same way. ■

## 5.2. Evolution of $(d+1)$ -tuple points

In Section 4.1 we have explained through formal calculations how the lower envelope equation (43)-(44) is obtained as a first-order approximation of the constitutive equations, defining the phases  $\Omega_k(\phi(t))$ ,  $k \in \mathcal{K}$ . Nevertheless, we need to verify that the lower envelope equation (43)-(44) indeed leads to the motion of  $(d+1)$ -tuple points with the expected velocity  $\theta$  in a neighbourhood of  $t = 0$ , under appropriate conditions on  $\phi$ . We prove indeed such a result in the following proposition, employing the implicit function theorem.

PROPOSITION 4 *Suppose  $\mathcal{I} = \mathcal{K}$ ,  $\kappa = d+1$ , and let  $\phi \in C^\infty([0, t_0] \times \mathbb{R}^d, \mathbb{R}^\kappa)$  be the solution to the lower envelope equation (43)-(44). Suppose  $D\hat{\phi}_{\mathcal{I}}(0, x)$  is invertible for all  $x \in \mathcal{M}_{\mathcal{I}}(\phi(0))$ , and  $\mathcal{M}_{\mathcal{I}}(\phi(0)) = \{\hat{x}\}$  consists of exactly one point. Then, upon reducing  $t_0 > 0$ , if necessary, there exists a unique smooth function  $\mathbf{x}^\dagger : [0, t_0] \rightarrow \mathbb{R}^d$  such that  $\{\mathbf{x}^\dagger(t)\} = \mathcal{E}_{\mathcal{I}}(\phi(t)) = \mathcal{M}_{\mathcal{I}}(\phi(t))$ , i.e.,  $\mathbf{x}^\dagger(t)$  is a  $(d+1)$ -tuple point for all  $t \in [0, t_0]$  in the sense of Definition 3. Also,  $\mathbf{x}^\dagger : [0, t_0] \rightarrow \mathbb{R}^d$  is the solution of*

$$\partial_t \mathbf{x}^\dagger(t) = \theta(\mathbf{x}^\dagger(t)), \quad \text{for all } t \in [0, t_0]$$

with the initial condition  $\mathbf{x}^\dagger(0) = \hat{x}$ .

PROOF Since  $\mathcal{I} = \mathcal{K}$ ,  $\kappa = d+1$ , and  $D\hat{\phi}_{\mathcal{I}}(0, x)$  is invertible for all  $x \in \mathcal{M}_{\mathcal{I}}(\phi(0))$ , there is that  $\mathcal{E}_{\mathcal{I}}(\phi(0)) = \mathcal{M}_{\mathcal{I}}(\phi(0))$  is a set of isolated points in view of Lemma 4. Without loss of generality, we can assume that  $\mathcal{M}_{\mathcal{I}}(\phi(0)) = \{\hat{x}\}$  is exactly one point.

We study the behaviour of  $\mathcal{M}_{\mathcal{I}}(\phi(t))$  for small  $t$ . In view of (10) we have

$$\mathcal{M}_{\mathcal{I}}(\phi(0)) = \{x \in \overline{\mathcal{D}} \mid \hat{\phi}_{\mathcal{I}}(0, x) = 0\} = \{\hat{x}\}.$$

Using the fact that  $D\widehat{\phi}_{\mathcal{I}}(0, x)$  is invertible for all  $x \in \mathcal{M}_{\mathcal{I}}(\phi(0))$ , and reducing  $t_0 > 0$ , if necessary, the implicit function theorem yields the existence of a unique smooth function  $\mathbf{x}^\dagger : [0, t_0] \rightarrow \mathbb{R}^d$ , such that  $\mathbf{x}^\dagger(0) = \hat{x}$  and  $\widehat{\phi}_{\mathcal{I}}(t, \mathbf{x}^\dagger(t)) = 0$  for all  $t \in [0, t_0]$ . Thus, we get

$$\{\mathbf{x}^\dagger(t)\} = \mathcal{M}_{\mathcal{I}}(\phi(t)) = \{x \in \overline{\mathcal{D}} \mid \widehat{\phi}_{\mathcal{I}}(t, x) = 0\}. \quad (48)$$

By reducing  $t_0 > 0$  again, if necessary, we also have that  $D\widehat{\phi}_{\mathcal{I}}(t, x)$  is invertible for all  $x \in \mathcal{M}_{\mathcal{I}}(\phi(t))$  and all  $t \in [0, t_0]$ . Thus, by applying Lemma 4 using  $\mathcal{I} = \mathcal{K}$  and  $\kappa = d + 1$ , we have  $\mathcal{E}_{\mathcal{I}}(\phi(t)) = \mathcal{M}_{\mathcal{I}}(\phi(t))$  and (48) yields that  $\mathbf{x}^\dagger(t)$  is a  $(d + 1)$ -tuple point for all  $t \in [0, t_0]$ . The implicit function theorem also yields for the derivative

$$\partial_t \widehat{\phi}_{\mathcal{I}}(t, \mathbf{x}^\dagger(t)) + D\widehat{\phi}_{\mathcal{I}}(t, \mathbf{x}^\dagger(t)) \partial_t \mathbf{x}^\dagger(t) = 0, \quad \text{for } t \in [0, t_0]. \quad (49)$$

Taking the difference between the equations for  $\phi_k$  and  $\phi_\ell$  at  $x = \mathbf{x}^\dagger(t)$  in (41), and subtracting the result to equation (49) yields

$$D\widehat{\phi}_{\mathcal{I}}(t, \mathbf{x}^\dagger(t))(\partial_t \mathbf{x}^\dagger(t) - \boldsymbol{\theta}(\mathbf{x}^\dagger(t))) = 0, \quad \text{for } t \in [0, t_0].$$

Using the fact that  $D\widehat{\phi}_{\mathcal{I}}(t, \mathbf{x}^\dagger(t))$  is invertible for  $t \in [0, t_0]$ , we get

$$\partial_t \mathbf{x}^\dagger(t) = \boldsymbol{\theta}(\mathbf{x}^\dagger(t)), \quad \text{for } t \in [0, t_0],$$

which proves the result. ■

We shall now discuss the case of  $\kappa = |\mathcal{K}| > d + 1$  and  $\mathcal{I} = \mathcal{K}$ . Let  $\phi \in \mathcal{C}^\infty([0, t_0] \times \mathbb{R}^d, \mathbb{R}^\kappa)$  be the solution to the lower envelope equation (43)-(44). Suppose that  $\mathcal{E}_{\mathcal{K}}(\phi(0)) \neq \emptyset$  and choose  $\hat{x} \in \mathcal{E}_{\mathcal{K}}(\phi(0))$ , then  $\hat{x}$  is at the junction of the  $\kappa$  phases  $\Omega_k(\phi(0))$ . Consider now the solution to the lower envelope equation, applied with  $\mathcal{K}^0 \subset \mathcal{K}$ , where  $|\mathcal{K}^0| = d + 1$ ,  $\mathcal{I}^0 = \mathcal{K}^0$ , and suppose that  $D\widehat{\phi}_{\mathcal{I}^0}(0, x)$  is invertible for all  $x \in \mathcal{M}_{\mathcal{I}^0}(\phi(0))$ . Then, we can apply Proposition 4 with  $\mathcal{I}^0$  and  $\mathcal{K}^0$ , which yields a smooth function  $\mathbf{x}_{\mathcal{K}^0}^\dagger : [0, t_0] \rightarrow \mathbb{R}^d$ , solution of

$$\partial_t \mathbf{x}_{\mathcal{K}^0}^\dagger(t) = \boldsymbol{\theta}(\mathbf{x}_{\mathcal{K}^0}^\dagger(t)), \quad \text{for all } t \in [0, t_0],$$

with the initial condition  $\mathbf{x}_{\mathcal{K}^0}^\dagger(0) = \hat{x}$ . Thus,  $\mathbf{x}_{\mathcal{K}^0}^\dagger$  is actually independent of  $\mathcal{K}^0$  (upon reducing  $t_0 > 0$ , if necessary) and we can use the notation  $\mathbf{x}^\dagger = \mathbf{x}_{\mathcal{K}^0}^\dagger$ . Also, by repeating the procedure for the entire subset of indices  $\mathcal{K}^0 \subset \mathcal{K}$ , satisfying  $|\mathcal{K}^0| = d + 1$ , we get  $\widehat{\phi}_{\mathcal{I}}(t, \mathbf{x}^\dagger(t)) = 0$  for all  $t \in [0, t_0]$ . Since  $\mathcal{I} = \mathcal{K}$ , this shows that  $\phi_k(t, \mathbf{x}^\dagger(t)) = \phi_\ell(t, \mathbf{x}^\dagger(t))$  for all  $k, \ell \in \mathcal{K}$  and  $t \in [0, t_0]$ , which means that  $\mathbf{x}^\dagger(t)$  is at the junction of the  $\kappa$  phases  $\Omega_k(\phi(t))$  for all  $t \in [0, t_0]$ . Thus, the interface point  $\hat{x}$  is also moving with the velocity  $\boldsymbol{\theta}$  on a sufficiently short time interval  $[0, t_0]$ , as in Proposition 4.

However, Example 4 and Fig. 2 demonstrate that when  $|\mathcal{K}| > d + 1$  and  $\mathcal{I} = \mathcal{K}$ , small random perturbations of  $\phi$  are likely to cause  $\hat{x}$  to split into multiple  $(d + 1)$ -tuple points, each moving in a different direction. Thus, from an implementation perspective, such points  $\hat{x}$  will probably be unstable and split from one iteration to the next one due to numerical errors.

## 6. Application to an inverse conductivity problem

### 6.1. Problem formulation

We consider the inverse problem of determining a matrix-valued conductivity  $\sigma$  within a body  $\mathcal{D} \subset \mathbb{R}^d$ , satisfying the elliptic equations

$$\operatorname{div}(\sigma \nabla y_i) = f \text{ in } \mathcal{D}, \quad (50)$$

which characterize the potentials  $y_i$ ,  $i = 1, \dots, m$ , associated with applied boundary current fluxes  $g_i = \sigma \nabla y_i \cdot \mathbf{n}|_{\partial \mathcal{D}}$ , and using measurements of boundary voltages  $h_i = y_i|_{\partial \mathcal{D}}$ , available on  $\partial \mathcal{D}$ .

With  $H_\diamond^1(\mathcal{D}) := \{v \in H^1(\mathcal{D}) : \int_{\mathcal{D}} v = 0\}$  and the compatibility condition

$$\int_{\mathcal{D}} f + \int_{\partial \mathcal{D}} g_i = 0, \quad (51)$$

the variational formulation reads: Find  $y_i \in H_\diamond^1(\mathcal{D})$  such that

$$\int_{\mathcal{D}} \sigma \nabla y_i \cdot \nabla v = \int_{\mathcal{D}} f v + \int_{\partial \mathcal{D}} g_i v, \quad \forall v \in H^1(\mathcal{D}). \quad (52)$$

When  $f \equiv 0$ , this problem is known as the continuum model in electrical impedance tomography (EIT), also known as the Calderón problem; we refer to the reviews by Bera (2018) and Borcea (2002), and the references therein. There exists a vast literature on EIT in the isotropic case, which corresponds to  $\sigma = \gamma I_d$ , where  $I_d$  is the identity matrix and  $\gamma$  is a scalar-valued function, but there are much less known results in the anisotropic case; however, one should mention the work of Alessandrini et al. (2018) for uniqueness results in the case of a layered anisotropic medium. Here, we compute the shape derivative in the multiphase anisotropic case, and for the numerics we focus on the isotropic case.

Let us introduce

$$\sigma = \sigma_\Omega := \sum_{k \in \mathcal{K}} \sigma_k \chi_{\Omega_k} \quad \text{and} \quad f = f_\Omega := \sum_{k \in \mathcal{K}} f_k \chi_{\Omega_k},$$

where  $\chi_{\Omega_k}$  denotes the characteristic function of  $\Omega_k$ ,  $\sigma_k$  are matrix-valued functions and  $\Omega \in \mathbb{P}_{\mathcal{K}}(\mathcal{D})$ ; see Definition 4.

ASSUMPTION 1 *Suppose  $\Omega \in \mathbb{P}_{\mathcal{K}}(\mathcal{D})$  and the following holds for all  $k \in \mathcal{K}$ :*

- $\sigma_k : \overline{\mathcal{D}} \rightarrow \mathbb{R}^{d \times d}$  is assumed to be in  $\mathcal{C}^1(\overline{\mathcal{D}}, \mathbb{R}^{d \times d})$  and uniformly positive definite, i.e., there exists  $\underline{\sigma}$  (independent of  $k$ ) such that  $\xi^\top \sigma_k(x) \xi \geq \underline{\sigma} |\xi|^2$  for a.e.  $x \in \overline{\mathcal{D}}$  and all  $\xi \in \mathbb{R}^d$ ,
- $f_k \in H^1(\mathcal{D})$ .

In order to obtain a numerical approximation of the solution to the EIT problem, we consider a Kohn-Vogelius approach with mixed boundary conditions as in Laurain and Sturm (2016). For  $i = 1, \dots, m$ , introduce  $u_i \in H_{a,h_i}^1(\mathcal{D})$  and  $v_i \in H_{b,h_i}^1(\mathcal{D})$ , solutions of

$$\int_{\mathcal{D}} \sigma_{\Omega} \nabla u_i \cdot \nabla w = \int_{\mathcal{D}} f_{\Omega} w + \int_{\Gamma_b} g_i w \quad \text{for all } w \in H_{a,0}^1(\mathcal{D}), \quad (53)$$

$$\int_{\mathcal{D}} \sigma_{\Omega} \nabla v_i \cdot \nabla w = \int_{\mathcal{D}} f_{\Omega} w + \int_{\Gamma_a} g_i w \quad \text{for all } w \in H_{b,0}^1(\mathcal{D}), \quad (54)$$

with  $\overline{\Gamma_a} \cup \overline{\Gamma_b} = \partial \mathcal{D}$ ,  $\Gamma_a \neq \emptyset$ ,  $\Gamma_b \neq \emptyset$ ,  $g_i \in L^2(\partial \mathcal{D})$ ,  $h_i \in H^{1/2}(\partial \mathcal{D})$  and

$$\begin{aligned} H_{a,h_i}^1(\mathcal{D}) &:= \{w \in H^1(\mathcal{D}) \mid w = h_i \text{ on } \Gamma_a\}, \\ H_{b,h_i}^1(\mathcal{D}) &:= \{w \in H^1(\mathcal{D}) \mid w = h_i \text{ on } \Gamma_b\}. \end{aligned}$$

The inverse problem then consists in finding  $\sigma_{\Omega}$  such that  $u_i = v_i$  for all  $i = 1, \dots, m$ . Indeed, if  $u_i = v_i$ , then, in view of (52),(53),(54), we get that  $u_i = v_i = y_i$  satisfies (50),  $\sigma \nabla y_i \cdot \mathbf{n}|_{\partial \mathcal{D}} = g_i$ , and  $y_i|_{\partial \mathcal{D}} = h_i$  since  $\overline{\Gamma_a} \cup \overline{\Gamma_b} = \partial \mathcal{D}$ , hence  $\sigma_{\Omega}$  is a solution of the inverse problem.

However, the measurements  $h_i$  are corrupted in practice by noise, and so we cannot expect that  $u_i = v_i$  be exactly achievable, but rather that  $|u_i - v_i|$  should be minimized. Thus, we shall consider the following multiphase cost functional:

$$\mathcal{J}(\Omega) := \frac{1}{2} \sum_{i=1}^m \int_{\mathcal{D}} (u_i - v_i)^2. \quad (55)$$

Note that  $u_i$  and  $v_i$  both depend on  $\Omega$ , but we use the notation  $u_i, v_i$  for simplicity.

## 6.2. Shape derivative of the cost functional

In this section we take  $m = 1$  and we write  $u, v, g, h$  instead of  $u_1, v_1, g_1, h_1$  to simplify the notation. The expression of the shape derivative of  $\mathcal{J}(\Omega)$  in (55) in the case of  $m > 1$  can be obtained straightforwardly by summing over  $i = 1, \dots, m$ .

Before stating the main result of this section, a short discussion about third-order tensors is useful. During the calculation of the shape derivative of  $\mathcal{J}(\Omega)$  the term appears

$$\tilde{\sigma}(t) := \sum_{k \in \mathcal{K}} \chi_{\Omega_k} \sigma_k \circ \Phi_t,$$

whose derivative at zero is given by

$$\tilde{\sigma}'(0) = \sum_{k \in \mathcal{K}} \chi_{\Omega_k} D\sigma_k \boldsymbol{\theta}.$$

Here,  $D\sigma_k : \mathcal{D} \rightarrow \mathbb{R}^{d \times d \times d}$  is a third-order tensor with entries  $(\partial_\ell(\sigma_k)_{ij})_{ij\ell}$ .

Let  $\mathbb{A} \in \mathbb{R}^{d \times d \times d}$  be a third-order tensor whose entries are denoted by  $\mathbb{A}_{ij\ell}$ . Then, for vectors  $y, z \in \mathbb{R}^d$ ,  $\mathbb{A}yz \in \mathbb{R}^d$  represents the vector with entries  $(\sum_{j,\ell=1}^d \mathbb{A}_{ij\ell} y_j z_\ell)_i$ . Let  $\mathbb{B} \in \mathbb{R}^{d \times d \times d}$  be another third-order tensor, satisfying

$$\mathbb{A}yz \cdot x = \mathbb{B}zx \cdot y \quad \text{for all } x, y, z \in \mathbb{R}^d.$$

Then we call  $\mathbb{B}$  the transpose of  $\mathbb{A}$  and write  $\mathbb{B} = \mathbb{A}^\top$ . It can be shown that the transpose of  $\mathbb{A}$  always exists and is unique; see Qi (2017, Proposition 3.1). Note that we have  $\mathbb{A}^{\top\top} = \mathbb{A}$ , but, in general,  $\mathbb{A}^{\top\top} \neq \mathbb{A}$ . For instance, the term  $D\sigma_k^\top \nabla u \nabla p \cdot \boldsymbol{\theta}$ , appearing in  $\mathbf{S}_0(\Omega) \cdot \boldsymbol{\theta}$  in (56), can be computed as follows:  $D\sigma_k^\top \nabla u \nabla p \cdot \boldsymbol{\theta} = D\sigma_k \boldsymbol{\theta} \nabla u \cdot \nabla p = \sum_{i,j,\ell=1}^d \partial_\ell(\sigma_k)_{ij} \boldsymbol{\theta}_\ell \partial_j u \partial_i p$ , which means that  $D\sigma_k^\top \nabla u \nabla p$  is a vector with entries  $(\sum_{i,j=1}^d \partial_\ell(\sigma_k)_{ij} \partial_j u \partial_i p)_\ell$ .

**THEOREM 4 (DISTRIBUTED SHAPE DERIVATIVE)** *Let Assumption 1 be satisfied, then the shape derivative of  $\mathcal{J}$  at  $\Omega$  in direction  $\boldsymbol{\theta} \in \mathcal{C}_{\partial\mathcal{D}}^1(\overline{\mathcal{D}}, \mathbb{R}^d)$  is given by*

$$d\mathcal{J}(\Omega)(\boldsymbol{\theta}) = \int_{\mathcal{D}} S_1(\Omega) : D\boldsymbol{\theta} + \mathbf{S}_0(\Omega) \cdot \boldsymbol{\theta} \, dx, \quad (56)$$

where  $S_1(\Omega) \in L^1(\mathcal{D}, \mathbb{R}^{d \times d})$  and  $\mathbf{S}_0(\Omega) \in L^1(\mathcal{D}, \mathbb{R}^d)$  are defined by

$$S_1(\Omega) = \left[ \frac{1}{2}(u-v)^2 - f_\Omega(p+q) + \sigma_\Omega \nabla u \cdot \nabla p + \sigma_\Omega \nabla v \cdot \nabla q \right] I_d \quad (57)$$

$$\begin{aligned} & - \nabla p \otimes \sigma_\Omega \nabla u - \nabla u \otimes \sigma_\Omega^\top \nabla p - \nabla q \otimes \sigma_\Omega \nabla v - \nabla v \otimes \sigma_\Omega^\top \nabla q, \\ \mathbf{S}_0(\Omega) &= \sum_{k \in \mathcal{K}} \chi_{\Omega_k} [D\sigma_k^\top \nabla u \nabla p + D\sigma_k^\top \nabla v \nabla q - (p+q) \nabla f_k], \end{aligned} \quad (58)$$

where  $D\sigma_k^\top$  denotes the transpose of the third-order tensor  $D\sigma_k : \mathcal{D} \rightarrow \mathbb{R}^{d \times d \times d}$ .

The adjoints  $p \in H_{a,0}^1(\mathcal{D})$  and  $q \in H_{b,0}^1(\mathcal{D})$  are the solutions of

$$\int_{\mathcal{D}} \sigma_\Omega^\top \nabla p \cdot \nabla w = - \int_{\mathcal{D}} (u-v)w \quad \text{for all } w \in H_{a,0}^1(\mathcal{D}), \quad (59)$$

$$\int_{\mathcal{D}} \sigma_\Omega^\top \nabla q \cdot \nabla w = \int_{\mathcal{D}} (u-v)w \quad \text{for all } w \in H_{b,0}^1(\mathcal{D}). \quad (60)$$

PROOF We use the averaged adjoint method from Sturm (2015) to compute the shape derivative of  $\mathcal{J}(\boldsymbol{\Omega})$ . The existence proof for the shape derivative of  $\mathcal{J}(\boldsymbol{\Omega})$  goes in a similar way as in Laurain and Sturm (2016), where the isotropic case for two phases was treated. Therefore, we only present a formal proof here, and we refer to Laurain and Sturm (2016) for more details on the verification of the assumptions of the averaged adjoint method.

First of all, in order to avoid working with  $H_{a,h}^1(\mathcal{D})$  and  $H_{b,h}^1(\mathcal{D})$ , we introduce alternative variational formulations, equivalent to (53)-(54): find  $u \in H^1(\mathcal{D})$  and  $v \in H^1(\mathcal{D})$ , the solutions to

$$\int_{\mathcal{D}} \sigma_{\Omega} \nabla u \cdot \nabla w = \int_{\mathcal{D}} f_{\Omega} w + \int_{\Gamma_b} g w + \int_{\Gamma_a} (\sigma_{\Omega}^{\top} \nabla w) \cdot \mathbf{n}(u - h) \text{ for all } w \in H_{a,0}^1(\mathcal{D}), \quad (61)$$

$$\int_{\mathcal{D}} \sigma_{\Omega} \nabla v \cdot \nabla w = \int_{\mathcal{D}} f_{\Omega} w + \int_{\Gamma_a} g w + \int_{\Gamma_b} (\sigma_{\Omega}^{\top} \nabla w) \cdot \mathbf{n}(v - h) \text{ for all } w \in H_{b,0}^1(\mathcal{D}). \quad (62)$$

Note that the integrals on  $\Gamma_a$  and  $\Gamma_b$  in (61)-(62) should be understood as dual products, since  $(\sigma_{\Omega}^{\top} \nabla w) \cdot \mathbf{n}$  belongs to  $H^{-1/2}(\partial\mathcal{D})$ . Compared to (53)-(54), the additional terms in (61)-(62) yield the non-homogeneous Dirichlet conditions  $u = h$  on  $\Gamma_a$  and  $v = h$  on  $\Gamma_b$ . While not identical, this reformulation of the problem bears similarities to the Nitsche method in the continuous setting; see Dumont et al. (2006) and Dupire et al. (2010).

We define the Lagrangian  $\mathcal{L} : \mathbb{P}_{\mathcal{K}}(\mathcal{D}) \times H^1(\mathcal{D}) \times H^1(\mathcal{D}) \times H_{a,0}^1(\mathcal{D}) \times H_{b,0}^1(\mathcal{D})$  as

$$\begin{aligned} \mathcal{L}(\boldsymbol{\Omega}, (\xi, \zeta), (\mu, \eta)) &:= \frac{1}{2} \int_{\mathcal{D}} (\xi - \zeta)^2 + \int_{\mathcal{D}} \sigma_{\Omega} \nabla \xi \cdot \nabla \mu \\ &\quad - \int_{\mathcal{D}} f_{\Omega} \mu - \int_{\Gamma_b} g \mu - \int_{\Gamma_a} (\sigma_{\Omega}^{\top} \nabla \mu) \cdot \mathbf{n}(\xi - h) \\ &\quad + \int_{\mathcal{D}} \sigma_{\Omega} \nabla \zeta \cdot \nabla \eta - \int_{\mathcal{D}} f_{\Omega} \eta - \int_{\Gamma_a} g \eta - \int_{\Gamma_b} (\sigma_{\Omega}^{\top} \nabla \eta) \cdot \mathbf{n}(\zeta - h). \end{aligned}$$

Then, the adjoints  $p \in H_{a,0}^1(\mathcal{D})$  and  $q \in H_{b,0}^1(\mathcal{D})$  are solutions to (see Laurain and Sturm, 2016)

$$\partial_{(\xi, \zeta)} \mathcal{L}(\boldsymbol{\Omega}, (u, v), (p, q))(\hat{\xi}, \hat{\zeta}) = 0 \quad \forall (\hat{\xi}, \hat{\zeta}) \in H^1(\mathcal{D}) \times H^1(\mathcal{D}).$$

This yields

$$\int_{\mathcal{D}} \sigma_{\Omega}^{\top} \nabla p \cdot \nabla \hat{\xi} = - \int_{\mathcal{D}} (u - v) \hat{\xi} + \int_{\Gamma_a} (\sigma_{\Omega}^{\top} \nabla p) \cdot \mathbf{n} \hat{\xi} \quad \text{for all } \hat{\xi} \in H^1(\mathcal{D}), \quad (63)$$

$$\int_{\mathcal{D}} \sigma_{\Omega}^{\top} \nabla q \cdot \nabla \hat{\zeta} = \int_{\mathcal{D}} (u - v) \hat{\zeta} + \int_{\Gamma_b} (\sigma_{\Omega}^{\top} \nabla q) \cdot \mathbf{n} \hat{\zeta} \quad \text{for all } \hat{\zeta} \in H^1(\mathcal{D}). \quad (64)$$

By taking test functions  $\hat{\xi} \in H_{a,0}^1(\mathcal{D}) \subset H^1(\mathcal{D})$  and  $\hat{\zeta} \in H_{b,0}^1(\mathcal{D}) \subset H^1(\mathcal{D})$  in (63)-(64), we get (59)-(60).

Following the averaged adjoint method, Laurain and Sturm (2016), we introduce the shape-Lagrangian  $G$  using a reparameterization of  $\mathcal{L}$ :

$$\begin{aligned} G(t, (\xi, \zeta), (\mu, \eta)) &:= \mathcal{L}(\Omega_t, (\xi, \zeta) \circ \Phi_t^{-1}, (\mu, \eta) \circ \Phi_t^{-1}) \\ &= \frac{1}{2} \int_{\mathcal{D}} (\xi^t - \zeta^t)^2 + \int_{\mathcal{D}} \sigma_{\Omega_t} D\Phi_t^{-\top} \circ \Phi_t^{-1}(\nabla \xi) \circ \Phi_t^{-1} \cdot D\Phi_t^{-\top} \circ \Phi_t^{-1}(\nabla \mu) \circ \Phi_t^{-1} \\ &\quad - \int_{\mathcal{D}} f_{\Omega_t} \mu^t - \int_{\Gamma_b} g\mu - \int_{\Gamma_a} (\sigma_{\Omega}^{\top} \nabla \mu) \cdot \mathbf{n}(\xi - h) \\ &\quad + \int_{\mathcal{D}} \sigma_{\Omega_t} D\Phi_t^{-\top} \circ \Phi_t^{-1}(\nabla \zeta) \circ \Phi_t^{-1} \cdot D\Phi_t^{-\top} \circ \Phi_t^{-1}(\nabla \eta) \circ \Phi_t^{-1} \\ &\quad - \int_{\mathcal{D}} f_{\Omega_t} \eta^t - \int_{\Gamma_a} g\eta - \int_{\Gamma_b} (\sigma_{\Omega}^{\top} \nabla \eta) \cdot \mathbf{n}(\zeta - h), \end{aligned}$$

with the notation  $\xi^t := \xi \circ \Phi_t^{-1}$  and a similar notation for the other functions involved. Note that we have used  $\Phi_t = \text{id}$  on  $\partial\mathcal{D}$ , where  $\text{id}$  denotes the identity mapping, due to  $\theta \in \mathcal{C}_{\partial\mathcal{D}}^1(\overline{\mathcal{D}}, \mathbb{R}^d)$ . Proceeding with the change of variables  $\mathbf{x} \mapsto \Phi_t(\mathbf{x})$  inside the integrals and using again  $\Phi_t = \text{id}$  on  $\partial\mathcal{D}$ , we get

$$\begin{aligned} G(t, (\xi, \zeta), (\mu, \eta)) &= \frac{1}{2} \int_{\mathcal{D}} (\xi - \zeta)^2 \det(\Phi_t) + \int_{\mathcal{D}} \mathbf{M}(t) \nabla \xi \cdot \nabla \mu \\ &\quad - \int_{\mathcal{D}} \tilde{f}(t) \mu \det(\Phi_t) - \int_{\Gamma_b} g\mu - \int_{\Gamma_a} (\sigma_{\Omega}^{\top} \nabla \mu) \cdot \mathbf{n}(\xi - h) \\ &\quad + \int_{\mathcal{D}} \mathbf{M}(t) \nabla \zeta \cdot \nabla \eta - \int_{\mathcal{D}} \tilde{f}(t) \eta \det(\Phi_t) \\ &\quad - \int_{\Gamma_a} g\eta - \int_{\Gamma_b} (\sigma_{\Omega}^{\top} \nabla \eta) \cdot \mathbf{n}(\zeta - h), \end{aligned}$$

where  $\mathbf{M}(t) := \det(\Phi_t) D\Phi_t^{-1} \tilde{\sigma}(t) D\Phi_t^{-\top}$ ,  $\tilde{\sigma}(t) := \sum_{k \in \mathcal{K}} \sigma_k \circ \Phi_t \chi_{\Omega_k}$ ,  $\tilde{f}(t) :=$

$\sum_{k \in \mathcal{K}} f_k \circ \Phi_t \chi_{\Omega_k}$ . We compute the derivatives at  $t = 0$ :

$$\begin{aligned}\tilde{f}'(0) &= \sum_{k \in \mathcal{K}} \chi_{\Omega_k} \nabla f_k \cdot \boldsymbol{\theta} \in L^2(\mathcal{D}), \\ \tilde{\sigma}'(0) &= \sum_{k \in \mathcal{K}} \chi_{\Omega_k} D\sigma_k \boldsymbol{\theta} \text{ with } D\sigma_k \boldsymbol{\theta} \in \mathcal{C}^0(\overline{\mathcal{D}}, \mathbb{R}^{d \times d}), \\ \mathbb{M}'(0) &= \operatorname{div}(\boldsymbol{\theta})\sigma_\Omega - D\boldsymbol{\theta}\sigma_\Omega - \sigma_\Omega D\boldsymbol{\theta}^\top + \tilde{\sigma}'(0).\end{aligned}$$

Note that  $D\sigma_k : \mathcal{D} \rightarrow \mathbb{R}^{d \times d \times d}$  is a third-order tensor, since  $\sigma_k$  are matrix-valued functions, and  $D\sigma_k \boldsymbol{\theta}$  is matrix-valued. According to the averaged adjoint method, see Laurain and Sturm (2016), the shape derivative  $d\mathcal{J}(\boldsymbol{\Omega})(\boldsymbol{\theta})$  is given by the derivative with respect to  $t$  of the shape-Lagrangian  $G$ , evaluated at the state  $(u, v)$  and adjoint state  $(p, q)$ , i.e.,

$$\begin{aligned}d\mathcal{J}(\boldsymbol{\Omega})(\boldsymbol{\theta}) &= \partial_t G(0, (u, v), (p, q)) \\ &= \frac{1}{2} \int_{\mathcal{D}} (u - v)^2 \operatorname{div}(\boldsymbol{\theta}) + \int_{\mathcal{D}} \mathbb{M}'(0) \nabla u \cdot \nabla p - \int_{\mathcal{D}} \tilde{f}'(0) p \\ &\quad + \int_{\mathcal{D}} f_\Omega p \operatorname{div}(\boldsymbol{\theta}) + \int_{\mathcal{D}} \mathbb{M}'(0) \nabla v \cdot \nabla q - \int_{\mathcal{D}} \tilde{f}'(0) q + \int_{\mathcal{D}} f_\Omega q \operatorname{div}(\boldsymbol{\theta}).\end{aligned}$$

Using tensor calculus, we compute

$$\begin{aligned}\mathbb{M}'(0) \nabla u \cdot \nabla p &= \operatorname{div}(\boldsymbol{\theta})\sigma_\Omega \nabla u \cdot \nabla p - D\boldsymbol{\theta}\sigma_\Omega \nabla u \cdot \nabla p - \sigma_\Omega D\boldsymbol{\theta}^\top \nabla u \cdot \nabla p + \tilde{\sigma}'(0) \nabla u \cdot \nabla p \\ &= (\sigma_\Omega \nabla u \cdot \nabla p) I_d : D\boldsymbol{\theta} - D\boldsymbol{\theta} : (\nabla p \otimes \sigma_\Omega \nabla u) - D\boldsymbol{\theta} : (\nabla u \otimes \sigma_\Omega^\top \nabla p) \\ &\quad + \sum_{k \in \mathcal{K}} \chi_{\Omega_k} D\sigma_k \boldsymbol{\theta} \nabla u \cdot \nabla p \\ &= D\boldsymbol{\theta} : [(\sigma_\Omega \nabla u \cdot \nabla p) I_d - \nabla p \otimes \sigma_\Omega \nabla u - \nabla u \otimes \sigma_\Omega^\top \nabla p] + \sum_{k \in \mathcal{K}} \chi_{\Omega_k} D\sigma_k^\top \nabla u \nabla p \cdot \boldsymbol{\theta},\end{aligned}$$

where  $D\sigma_k^\top$  denotes the transpose of the third-order tensor  $D\sigma_k$ . The other terms of  $d\mathcal{J}(\boldsymbol{\Omega})(\boldsymbol{\theta})$  can be rearranged in a similar way to obtain (56). ■

**REMARK 1** Formula (56) generalizes Laurain and Sturm (2016, Proposition 6.2) when the same cost functional (55) is used (this corresponds to taking  $\alpha_1 = 1$  and  $\alpha_2 = 0$  in Laurain and Sturm (2016, Proposition 6.2)). To be more precise, the result of Laurain and Sturm (2016, Proposition 6.2) can be recovered by taking two phases ( $\mathcal{K} = \{0, 1\}$ ) and  $\sigma_\Omega = \sigma_0 \chi_{\Omega_0} + \sigma_1 \chi_{\Omega_1}$ , where  $\sigma_0, \sigma_1$  are multiples of the identity matrix.

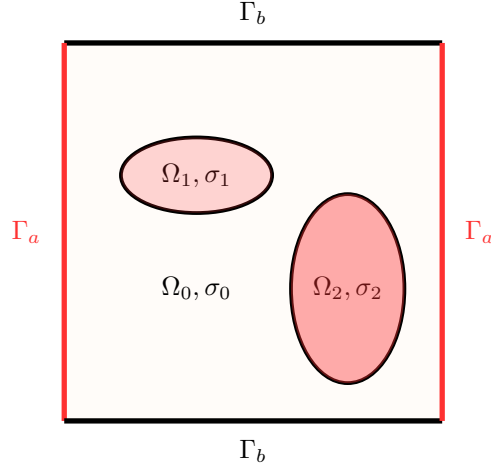


Figure 4: Example of partition  $\bar{\mathcal{D}} = \bar{\Omega}_0 \cup \bar{\Omega}_1 \cup \bar{\Omega}_2$  and boundaries  $\Gamma_a = \Gamma_{\text{left}} \cup \Gamma_{\text{right}}$ ,  $\Gamma_b = \Gamma_{\text{lower}} \cup \Gamma_{\text{upper}}$

### 6.3. The algorithm and numerical results

Without loss of generality, we take  $\phi_0 \equiv 0$  in the numerics. The phases  $\Omega_k(\phi(t))$  are defined as in (2). We consider the particular case of  $\kappa = 3$ ,  $\mathcal{K} = \{0, 1, 2\}$ ,  $d = 2$ , which corresponds to three phases in two dimensions. We choose  $\mathcal{D} = (0, 1) \times (0, 1)$ ,  $f_{\Omega} \equiv 0$  and  $\sigma_{\Omega} = \sigma_0 \chi_{\Omega_0} + \sigma_1 \chi_{\Omega_1} + \sigma_2 \chi_{\Omega_2}$ , where  $\sigma_k = \sigma_{k,0} I_d$  for  $k \in \mathcal{K}$ , and  $\sigma_{k,0}$  are known scalar values. This corresponds to the isotropic EIT case, and (57)-(58) become in this case

$$\begin{aligned} S_1(\Omega) &= \left[ \frac{1}{2}(u-v)^2 + \sigma_{\Omega} \nabla u \cdot \nabla p + \sigma_{\Omega} \nabla v \cdot \nabla q \right] I_d \\ &\quad - 2\sigma_{\Omega} [\nabla u \odot \nabla p + \nabla v \odot \nabla q], \\ S_0(\Omega) &\equiv 0, \end{aligned}$$

where  $\nabla u \odot \nabla p := (\nabla u \otimes \nabla p + \nabla p \otimes \nabla u)/2$ .

We use the software package FEniCS for the implementation; see Logg, Mardal and Wells (2012). Our algorithm closely follows the ideas of Laurain (2018), where a distributed shape derivative-based FEniCS implementation was described for the level set method. Thus, we explain here the main principles of our implementation and refer to Laurain (2018) for detailed explanations. To solve the lower envelope equation (43)-(44),  $\mathcal{D} = (0, 1) \times (0, 1)$  is discretized using a regular grid. The node coordinates are given by  $(ih, jh)$ ,  $0 \leq i, j \leq N + 1$ ,

where  $h = 1/N$  is the discretization step. In our numerical experiments we take  $N = 255$ . The lower envelope function  $\phi$  is then solved on this grid using the same Lax-Friedrichs flux as described in Laurain (2018, Section 5.2). Concerning the “freezing” of  $\theta$ , explained in Section 4.4, we follow the heuristics of Laurain (2018) and take 10 pseudo-time steps in the update of the lower envelope equation (43)-(44) to accelerate the convergence.

To solve the PDEs for the states (53),(54) and adjoint states (59),(60), the square  $\mathcal{D}$  is discretized using the FEniCS built-in mesh `RectangleMesh`, which generates a regular triangulation by subdividing each quadrilateral element of a Cartesian grid into two triangles. We take  $N = 255$  cells in both directions and the default direction “right” for the diagonal. We then use standard piecewise linear Lagrange elements, accessible in FEniCS via the built-in `FunctionSpace(mesh, "Lagrange", 1)`.

In our numerical experiments, we choose  $\sigma_{0,0} = 1$ ,  $\sigma_{1,0} = 3$ ,  $\sigma_{2,0} = 15$ . We choose  $\Gamma_a = \Gamma_{\text{left}} \cup \Gamma_{\text{right}}$  with  $\Gamma_{\text{left}} = \{0\} \times [0, 1]$ ,  $\Gamma_{\text{right}} = \{1\} \times [0, 1]$  and  $\Gamma_b = \Gamma_{\text{lower}} \cup \Gamma_{\text{upper}}$  with  $\Gamma_{\text{lower}} = [0, 1] \times \{0\}$ ,  $\Gamma_{\text{upper}} = [0, 1] \times \{1\}$ ; see Fig. 4. We also normalize the cost function (55) and the associated shape derivative by dividing each term in the sum over  $i = 1, \dots, m$ , by the constant  $\frac{1}{2} \int_{\mathcal{D}} (u_i^{(0)} - v_i^{(0)})^2$ , where  $u_i^{(0)}, v_i^{(0)}$  represent  $u_i$  and  $v_i$ , computed for the initial partition  $\Omega^{(0)}$ .

Synthetic measurements  $h_i$  are obtained by taking the trace on  $\partial\mathcal{D}$  of the solution to (50) using a ground truth partition  $\Omega^*$ ,  $f_{\Omega^*} \equiv 0$  and known currents  $g_i$ ,  $i = 1, \dots, m$ . To simulate the noisy EIT data, each measurement  $h_i$  is corrupted by adding a normal Gaussian noise with mean zero and standard deviation  $\delta \|h_i\|_{\infty}$ , where  $\delta$  is a parameter. The noise level is computed as

$$\text{noise} = \frac{\sum_{i=1}^m \|h_i - \tilde{h}_i\|_{L^2(\partial\mathcal{D})}}{\sum_{i=1}^m \|h_i\|_{L^2(\partial\mathcal{D})}}, \quad (65)$$

where  $h_i$  and  $\tilde{h}_i$  are, respectively, the noiseless and noisy measurements, corresponding to the current  $g_i$ .

In the numerical tests, we use  $m = 11$  measurements and define the currents in the following way:

$$\begin{aligned} g_1 &= 1 \text{ on } \Gamma_{\text{left}} \cup \Gamma_{\text{right}} \text{ and } g_1 = -1 \text{ on } \Gamma_{\text{upper}} \cup \Gamma_{\text{lower}}, \\ g_2 &= 1 \text{ on } \Gamma_{\text{left}} \cup \Gamma_{\text{upper}} \text{ and } g_2 = -1 \text{ on } \Gamma_{\text{right}} \cup \Gamma_{\text{lower}}, \\ g_3 &= 1 \text{ on } \Gamma_{\text{left}} \cup \Gamma_{\text{lower}} \text{ and } g_3 = -1 \text{ on } \Gamma_{\text{right}} \cup \Gamma_{\text{upper}}. \end{aligned}$$

Then we choose

$$g_4 = \arctan(500(x_2 - 0.5)) \text{ on } \Gamma_{\text{left}} \text{ and } g_4 = 0 \text{ otherwise,}$$

which is used as an approximation of the function

$$g = \frac{\pi}{2} \text{ on } \Gamma_{\text{left}} \cap \{x_2 > 0.5\}, \quad g = -\frac{\pi}{2} \text{ on } \Gamma_{\text{left}} \cap \{x_2 \leq 0.5\}$$

and  $g_4 = 0$  otherwise,

and  $g_5, g_6, g_7$  are defined similarly as  $g_4$  on  $\Gamma_{\text{right}}, \Gamma_{\text{upper}}, \Gamma_{\text{lower}}$ , respectively. Then

$$g_8 = \sin(4\pi x_2) \text{ on } \Gamma_{\text{left}} \text{ and } g_8 = 0 \text{ otherwise,}$$

and  $g_9, g_{10}, g_{11}$  are defined in a similar way on  $\Gamma_{\text{right}}, \Gamma_{\text{upper}}, \Gamma_{\text{lower}}$ , respectively.

In order to obtain the descent direction, we solve

$$\mathcal{B}(\boldsymbol{\theta}, \boldsymbol{\xi}) := \int_{\mathcal{D}} \alpha_1 D\boldsymbol{\theta} : D\boldsymbol{\xi} + \alpha_2 \boldsymbol{\theta} \cdot \boldsymbol{\xi} + \int_{\partial\mathcal{D}} \alpha_3 \boldsymbol{\theta} \cdot \boldsymbol{\xi} = -d\mathcal{J}(\boldsymbol{\Omega})(\boldsymbol{\xi}) \quad (66)$$

for all  $\boldsymbol{\xi} \in H^1(\mathcal{D})^2$ ,

with  $\alpha_1 > 0, \alpha_2 > 0$  and  $\alpha_3 > 0$ . This procedure has been introduced and developed in Burger (2003) and de Gournay (2006), see also Allaire, Dapogny and Jouve (2021), using the boundary expression of the shape derivative, such as (34), on the right-hand side of (66), for the purpose of regularizing  $\boldsymbol{\theta}$  and extending it to  $\mathcal{D}$ . Here, we employ the same procedure, but with the distributed shape derivative (56) on the right-hand side of (66). It is particularly useful in the case of the distributed shape derivative, as there is no straightforward way of obtaining a descent direction using (56) directly, due to the term  $D\boldsymbol{\theta}$ . The solution  $\boldsymbol{\theta}$  of (66) is defined on all of  $\mathcal{D}$  and is a descent direction, since  $dJ(\boldsymbol{\Omega})(\boldsymbol{\theta}) = -\mathcal{B}(\boldsymbol{\theta}, \boldsymbol{\theta}) < 0$  if  $\boldsymbol{\theta} \neq 0$ . In our experiment, we used  $\alpha_1 = 0.2, \alpha_2 = 0.8$  and  $\alpha_3 = 10^5$ . The role of the large coefficient  $\alpha_3$  is to provide a relaxation of the Dirichlet boundary condition  $\boldsymbol{\theta} \in \mathcal{C}_{\partial\mathcal{D}}^1(\overline{\mathcal{D}}, \mathbb{R}^d)$ , so that slow tangential displacements of the phases can occur on  $\partial\mathcal{D}$ , which allows us to consider discontinuities of the conductivity  $\sigma_{\boldsymbol{\Omega}}$  up to the boundary  $\partial\mathcal{D}$ . To compute the descent direction numerically, we integrate separately on the subdomains  $\Omega_0, \Omega_1, \Omega_2$ , due to the discontinuous conductivity  $\sigma_{\boldsymbol{\Omega}}$  appearing in the distributed shape derivative (56). Numerically, we employ the built-in FEniCS class `Subdomain` for this purpose, which requires the lower envelope functions  $\phi_1, \phi_2$  in the finite element space of piecewise linear elements. Since the Cartesian grid aligns with the vertices of the finite element mesh, this is performed without introducing additional numerical errors by projecting  $\phi_1, \phi_2$ , which are computed on the Cartesian grid, onto the finite element space. We refer to Laurain (2018, Section 6) for detailed explanations about the numerical implementation of the descent direction in a similar framework.

We define a relative error measure for the reconstruction as (note that  $E(\boldsymbol{\Omega})$

is a percentage)

$$E(\Omega) := 100 \times \frac{\int_{\mathcal{D}} |\sigma_{\Omega} - \sigma_{\Omega^*}|}{\int_{\mathcal{D}} |\sigma_{\Omega}|}.$$

Numerical results are shown in Fig. 5. The ground truth conductivity  $\sigma_{\Omega^*}$  is composed of a background with two low conductivity phases,  $\sigma_{0,0} = 1$  and  $\sigma_{1,0} = 3$ , separated by a curvy horizontal interface, and of two inclusions of different sizes and higher conductivity  $\sigma_{2,0} = 15$  (see the ground truth  $\sigma_{\Omega^*}$  in Fig. 5). The goal is to reconstruct the shapes of the two inclusions and the location of the interface between the two low conductivity phases. As can be seen in Fig. 5, the shapes of the two inclusions are well reconstructed albeit slightly smoothed. The interface between the two weak phases is well reconstructed in the regions closer to the boundary, and less so in the center, as expected for this type of inverse problem. Indeed, we emphasize that the EIT problem is severely ill-posed, see Borcea (2002), imposing an inherent limitation on the achievable quality of reconstruction, regardless of the reconstruction method used.

In Fig. 5, the sensitivity of the reconstruction with respect to noise is illustrated. Numerical results corresponding to three different noise levels are compared. In the three cases, the reconstruction is able to capture the main geometric features of the ground truth. The relative errors at the final iteration, corresponding to the noise levels 0%, 1.02% and 2.03%, are given by  $E(\Omega^{\text{rec}}) = 5.72\%$ ,  $6.19\%$  and  $6.81\%$ , respectively, thus showing that the method is robust with respect to noise.

## Acknowledgments

The author would like to thank Professor James A. Sethian for the discussion about the tracking of interfaces in multiphase problems and the inspiration to work on this topic.

## Funding

The author gratefully acknowledges the support of the Brazilian National Council for Scientific and Technological Development (Conselho Nacional de Desenvolvimento Científico e Tecnológico - CNPq) through the process: 408175/2018-4 “Otimização de forma não suave e controle de problemas de fronteira livre”, and through the program “Bolsa de Produtividade em Pesquisa - PQ 2018”, process: 304258/2018-0.

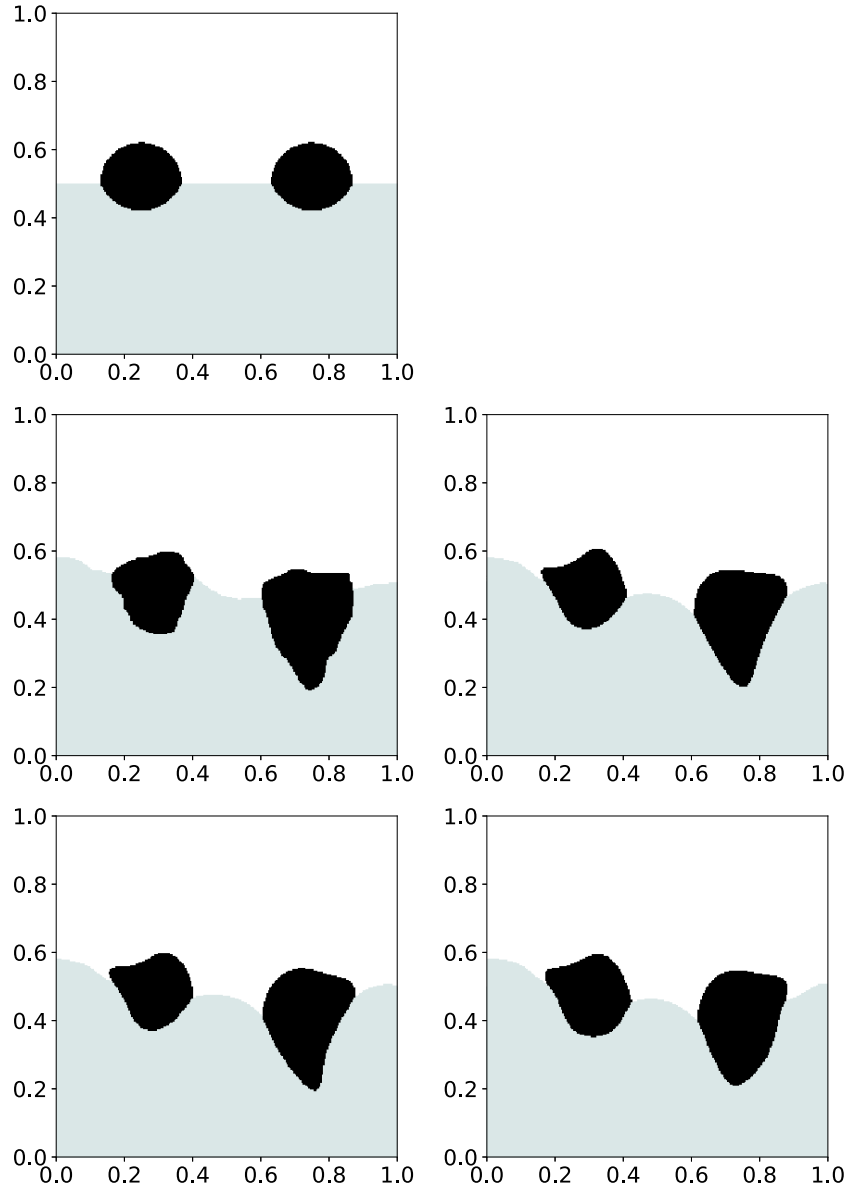


Figure 5: Initialization (first row), ground truth  $\sigma_{\Omega^*}$  (second row left), reconstructions  $\sigma(\Omega^{\text{rec}})$  using 11 boundary currents with 0% noise and  $E(\Omega^{\text{rec}}) = 5.72\%$  error (second row right), with 1.02% noise and  $E(\Omega^{\text{rec}}) = 6.19\%$  error (third row left), with 2.03% noise and  $E(\Omega^{\text{rec}}) = 6.81\%$  error (third row right). The conductivity values are  $\sigma_{0,0} = 1$  (white),  $\sigma_{1,0} = 3$  (light gray),  $\sigma_{2,0} = 15$  (black).

## References

- ALBUQUERQUE, Y. F., LAURAIN, A. AND STURM, K. (2020) A shape optimization approach for electrical impedance tomography with point measurements. *Inverse Problems*, **36**(9): 095006, 27.
- ALESSANDRINI, G., DE HOOP, M. V., GABURRO, R. AND SINCICH, E. (2018) EIT in a layered anisotropic medium. *Inverse Probl. Imaging*, **12**(3): 667–676.
- ALLAIRE, G., DAPOGNY, C., DELGADO, G. AND MICHAELIDIS, G. (2014) Multi-phase structural optimization via a level set method. *ESAIM Control Optim. Calc. Var.*, **20**(2): 576–611.
- ALLAIRE, G., DAPOGNY, C., AND JOUVE, F. C. (2021) Shape and topology optimization. In: *Geometric Partial Differential Equations. Part II. Handb. Numer. Anal.*, 1–132. Elsevier/North-Holland, Amsterdam.
- AZEGAMI, H. (2020) *Shape Optimization Problems. Springer Optimization and Its Applications* **164**. Springer, Singapore.
- BARRETT, J. W., GARCKE, H., AND NÜRNBERG, R. (2008) On sharp interface limits of Allen-Cahn/Cahn-Hilliard variational inequalities. *Discrete Contin. Dyn. Syst. Ser. S*, **1**(1): 1–14.
- BERA, T. K. (2018) Applications of electrical impedance tomography (EIT): A short review. *IOP Conference Series: Materials Science and Engineering*, **331**: 012004.
- BERETTA, E., FRANCINI, E. AND VESSELLA, S. (2017) Differentiability of the Dirichlet to Neumann map under movements of polygonal inclusions with an application to shape optimization. *SIAM J. Math. Anal.*, **49**(2): 756–776.
- BERETTA, E., MICHELETTI, S., PEROTTO, S. AND SANTACESARIA, M. (2018) Reconstruction of a piecewise constant conductivity on a polygonal partition via shape optimization in EIT. *J. Comput. Phys.*, **353**: 264–280.
- BIRGIN, E. G., LAURAIN, A. AND MENEZES, T. C. (2023) Sensitivity analysis and tailored design of minimization diagrams. *Mathematics of Computation*, **92**(344): 2715–2768.
- BORCEA, L. (2002) Electrical impedance tomography. *Inverse Problems*, **18**(6): R99–R136.
- BRONSARD, L., GARCKE, H. AND STOTH, B. (1998) A multi-phase Mullins-Sekerka system: matched asymptotic expansions and an implicit time discretisation for the geometric evolution problem. *Proc. Roy. Soc. Edinburgh Sect. A*, **128**(3): 481–506.
- BRONSARD, L. AND WETTON, B. T. R. (1995) A numerical method for tracking curve networks moving with curvature motion. *J. Comput. Phys.*, **120**(1): 66–87.

- BURGER, M. (2003) A framework for the construction of level set methods for shape optimization and reconstruction. *Interfaces Free Bound.*, **5**(3): 301–329.
- CHEN, S., GONELLA, S., CHEN, W. AND LIU, W. K. (2010) A level set approach for optimal design of smart energy harvesters. *Comput. Methods Appl. Mech. Engrg.*, **199**(37-40): 2532–2543.
- DE GOURNAY, F. (2006) Velocity extension for the level-set method and multiple eigenvalues in shape optimization. *SIAM J. Control Optim.*, **45**(1): 343–367.
- DELFOUR, M., PAYRE, G. AND ZOLÉSIO, J.-P. (1985) An optimal triangulation for second-order elliptic problems. *Comput. Methods Appl. Mech. Engrg.*, **50**(3): 231–261.
- DELFOUR, M. C. AND ZOLÉSIO, J.-P. (2011) *Shapes and Geometries. Advances in Design and Control 22*. Society for Industrial and Applied Mathematics (SIAM), Philadelphia, PA, second edition.
- DUMONT, S., GOUBET, O., HA-DUONG, T. AND VILLON, P. (2006) Meshfree methods and boundary conditions. *Internat. J. Numer. Methods Engrg.*, **67**(7): 989–1011.
- DUPIRE, G., BOUFFLET, J. P., DAMBRINE, M. AND VILLON, P. (2010) On the necessity of Nitsche term. *Appl. Numer. Math.*, **60**(9): 888–902.
- EDELSBRUNNER, H. AND SEIDEL, R. (1986) Voronoi diagrams and arrangements. *Discrete & Computational Geometry*, **1**(1): 25–44.
- GARCKE, H., NESTLER, B. AND STOTH, B. (2000) A multiphase field concept: numerical simulations of moving phase boundaries and multiple junctions. *SIAM J. Appl. Math.*, **60**(1): 295–315.
- GIBOU, F., FEDKIW, R. AND OSHER, S. (2018) A review of level-set methods and some recent applications. *Journal of Computational Physics*, **353**: 82–109.
- HINTERMÜLLER, M. AND LAURAIN, A. (2008) Electrical impedance tomography: from topology to shape. *Control Cybernet.*, **37**(4): 913–933.
- HINTERMÜLLER, M. AND LAURAIN, A. (2009) Multiphase image segmentation and modulation recovery based on shape and topological sensitivity. *J. Math. Imaging Vision*, **35**(1): 1–22.
- HINTERMÜLLER, M., LAURAIN, A. AND NOVOTNY, A. A. (2012) Second-order topological expansion for electrical impedance tomography. *Adv. Comput. Math.*, **36**(2): 235–265.
- HIPTMAIR, R., PAGANINI, A. AND SARGHEINI, S. (2014) Comparison of approximate shape gradients. *BIT Numerical Mathematics*, **55**(2): 459–485.
- LAMBOLEY, J. AND PIERRE, M. (2007) Structure of shape derivatives around irregular domains and applications. *J. Convex Anal.*, **14**(4): 807–822.

- LAURAIN, A. (2017) Stability analysis of the reconstruction step of the voronoi implicit interface method. *SIAM Journal on Numerical Analysis*, **55**(1): 1–30.
- LAURAIN, A. (2018) A level set-based structural optimization code using FEniCS. *Structural and Multidisciplinary Optimization*, **58**(3): 1311–1334.
- LAURAIN, A. (2020) Distributed and boundary expressions of first and second order shape derivatives in nonsmooth domains. *Journal de Mathématiques Pures et Appliquées*, **134**, 328–368.
- LAURAIN, A. AND STURM, K. (2016) Distributed shape derivative via averaged adjoint method and applications. *ESAIM Math. Model. Numer. Anal.*, **50**(4): 1241–1267.
- LI, H. AND TAI, X.-C. (2007) Piecewise constant level set method for multiphase motion. *Int. J. Numer. Anal. Model.*, **4**(2): 291–305.
- LIU, D., KHAMBAMPATI, A. K., KIM, S. AND KIM, K. Y. (2015) Multiphase flow monitoring with electrical impedance tomography using level set based method. *Nuclear Engineering and Design*, 289: 108–116.
- LIU, D., ZHAO, Y., KHAMBAMPATI, A. K., SEPPÄNEN, A. AND DU, J. (2018) A parametric level set method for imaging multiphase conductivity using electrical impedance tomography. *IEEE Transactions on Computational Imaging*, **4**(4): 552–561.
- LOGG, A., MARDAL, K.-A. AND WELLS, G. N., EDS. (2012) *Automated Solution of Differential Equations by the Finite Element Method. Lecture Notes in Computational Science and Engineering*, **84**, Springer.
- MEI, Y. AND WANG, X. (2004) A level set method for structural topology optimization with multi-constraints and multi-materials. *Acta Mech. Sin. Engl. Ser.*, **20**(5): 507–518.
- MERRIMAN, B., BENCE, J. K. AND OSHER, S. J. (1994) Motion of multiple functions: a level set approach. *J. Comput. Phys.*, **112**(2): 334–363.
- NOH, W. AND WOODWARD, P. (1976) Slic (simple line interface calculation). In: A. van de Vooren and P. Zandbergen, eds., *Proceedings of the Fifth International Conference on Numerical Methods in Fluid Dynamics June 28–July 2, 1976 Twente University, Enschede, Lecture Notes in Physics*, **59**, 330–340. Springer, Berlin Heidelberg.
- OSHER, S. AND FEDKIW, R. (2003) Level set methods and dynamic implicit surfaces, *Applied Mathematical Sciences*, **153** Springer-Verlag, New York.
- OSHER, S. AND SETHIAN, J. A. (1988) Fronts propagating with curvature-dependent speed: algorithms based on Hamilton-Jacobi formulations. *J. Comput. Phys.*, **79**(1): 12–49.
- QI, L. (2017) Transposes, L-eigenvalues and invariants of third order tensors. arXiv preprint 1704.01327.

- SAYE R. I. AND SETHIAN, J. A. (2011) The Voronoi implicit interface method for computing multiphase physics. *Proc. Natl. Acad. Sci. USA*, **108**(49): 19498–19503.
- SAYE, R. I. AND SETHIAN, J. A. (2013) Multiscale modeling of membrane rearrangement, drainage, and rupture in evolving foams. *Science*, **340**(6133): 720–724.
- SETHIAN, J. A. (1999) *Level Set Methods and Fast Marching Methods*. Cambridge Monographs on Applied and Computational Mathematics, **3**. Cambridge University Press, Cambridge, second edition.
- SMITH, K. A., SOLIS, F. J. AND CHOPP, D. L. (2002) A projection method for motion of triple junctions by levels sets. *Interfaces Free Bound.*, **4**(3): 263–276.
- SOKOLOWSKI, J. AND ZOLÉSIO, J.-P. (1992) *Introduction to Shape Optimization*. Springer Series in Computational Mathematics, **16**, Springer-Verlag, Berlin.
- STURM, K. (2015) Minimax Lagrangian approach to the differentiability of nonlinear PDE constrained shape functions without saddle point assumption. *SICON*, **53**(4): 2017–2039.
- STURM, K. (2016) A structure theorem for shape functions defined on sub-manifolds. *Interfaces Free Bound.*, **18**(4): 523–543.
- TAI, X.-C. AND CHAN, T. F. (2004) A survey on multiple level set methods with applications for identifying piecewise constant functions. *Int. J. Numer. Anal. Model.*, **1**(1): 25–47.
- TAVAKOLI, R. AND MOHSENI, S. M. (2014) Alternating active-phase algorithm for multimaterial topology optimization problems: a 115-line MATLAB implementation. *Struct. Multidiscip. Optim.*, **49**(4): 621–642.
- TOSSAVAINEN, O.-P., VAUHKONEN, M., KOLEHMAINEN, V. AND YOUNG KIM, K. (2006) Tracking of moving interfaces in sedimentation processes using electrical impedance tomography. *Chemical Engineering Science*, **61**(23): 7717–7729.
- VESE, L. A. AND CHAN, T. F. (2002) A multiphase level set framework for image segmentation using the mumford and shah model. *International Journal of Computer Vision*, **50**(3): 271–293.
- VOGIATZIS, P., CHEN, S., WANG, X., LI, T. AND WANG, L. (2017) Topology optimization of multi-material negative Poisson’s ratio metamaterials using a reconciled level set method. *Comput.-Aided Des.*, **83**: 15–32.
- WANG, M. Y. AND WANG, X. (2004) “Color” level sets: a multi-phase method for structural topology optimization with multiple materials. *Comput. Methods Appl. Mech. Engrg.*, **193**(6-8): 469–496.
- WANG, Y., LUO, Z., KANG, Z. AND ZHANG, N. (2015) A multi-material level set-based topology and shape optimization method. *Comput. Methods Appl. Mech. Engrg.*, **283**: 1570–1586.

- WEAIRE, D. AND HUTZLER, S. (1999) *The Physics of Foams*. Clarendon Press.
- ZHANG, X., CHEN, J.-S. AND OSHER, S. (2008) A multiple level set method for modeling grain boundary evolution of polycrystalline materials. *Interaction and Multiscale Mechanics*, **1**(2): 191–209.
- ZHAO, H.-K., CHAN, T., MERRIMAN, B. AND OSHER, S. (1996) A variational level set approach to multiphase motion. *J. Comput. Phys.*, **127**(1): 179–195.
- ZOLÉSIO, J.-P. (1979) *Identification de domaines par déformations*. Thèse de doctorat d'état, Université de Nice, France.
- ZUO, W. AND SAITOU, K. (2017) Multi-material topology optimization using ordered SIMP interpolation. *Struct. Multidiscip. Optim.*, **55**(2): 477–491.